ERDC/CERL TR-04-6

US Army Corps of Engineers®
Engineer Research and Development Center

Tri-Directional Seismic Analysis of an Unreinforced Masonry Building With Flexible Diaphragms

Steven C. Sweeney, Matthew A. Horney, and Sarah L. Orton

April 2004

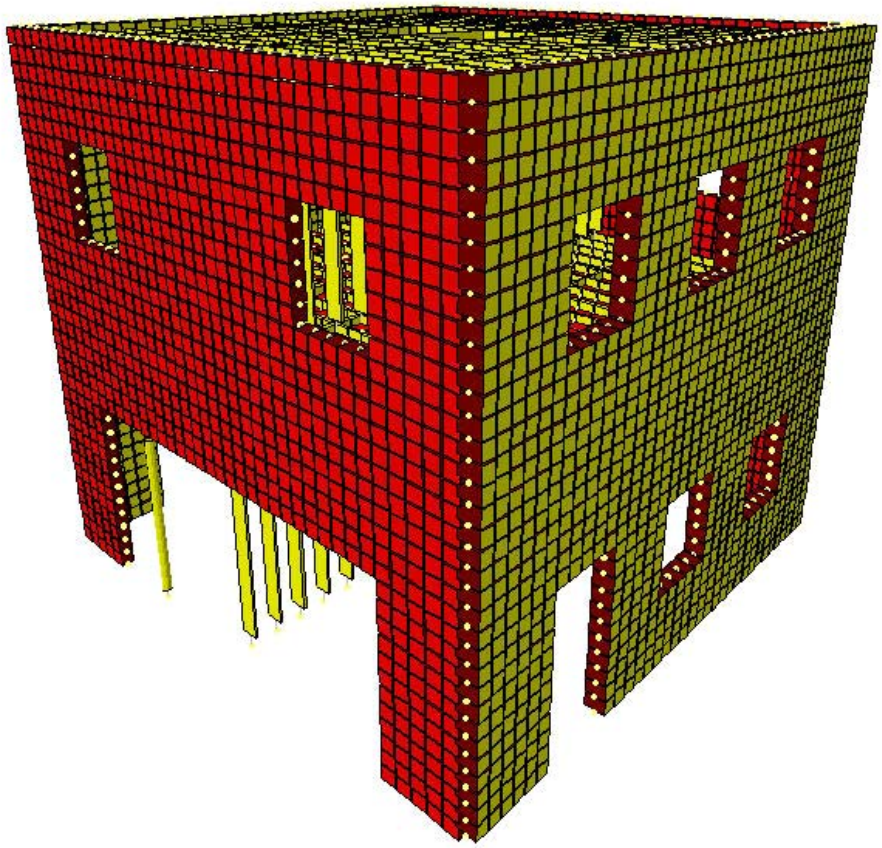

Construction Engineering Research Laboratory

ERDC/CERL TR-04-6
April 2004

Tri-Directional Seismic Analysis of an Unreinforced Masonry Building With Flexible Diaphragms

Steven C. Sweeney, Matthew A. Horney, and Sarah L. Orton

Final Report

Prepared for U.S. Army Corps of Engineers
Washington, DC 20314-1000

ABSTRACT: To understand the susceptibility that buildings with flexible diaphragm systems have to earthquakes, their seismic response to tri-axial base motions is assessed. The research centers on a tri-directional analytical study of a two-story half-scale unreinforced masonry (URM) structure. The study investigates the effect of tri-axial base motions on response of the structure. It determines how individual component behavior, such as a pier or floor diaphragm, affects the behavior of the entire building system. This project achieves a greater understanding of the tri-directional seismic response of URM building systems with flexible diaphragms.

Analysis is conducted on the components of the structure and the building system. The masonry piers and the wood diaphragms are analyzed to determine component behaviors. The building system is analyzed using equivalent static, response spectrum, linear time history, and pushover analysis. Each analysis method includes careful consideration of the directions of load application. Seismic loads are applied independently along each coordinate axis and simultaneously along all three directions.

Evaluations of the response of the building system under tri-directional loads found that simultaneous tri-directional seismic motions do influence the response of the building system. Maximum responses for two or more directional components can combine to produce a result greater than if a single direction were considered. Furthermore, the interconnectivity of walls in a masonry box building may cause significant changes in wall vertical forces due to global overturning of the building. This change in vertical force and combined base shears can occur simultaneously leading to significant damage in a building whose lateral resistance is highly dependant on the vertical compressive stress.

Contents

List of Figures and Tables

Figures

Tables

Conversion Factors

Non-SI* units of measurement used in this report can be converted to SI units as follows:

Multiply	By	To Obtain
feet	0.3048	meters
inches	0.0254	meters
kips per square foot	47.88026	kilopascals
kips per square inch	6.894757	megapascals
psf	47.880	pascals
pounds (force) per square inch	0.006894757	megapascals
pounds (mass)	0.4535924	kilograms

*_Système International d'Unités_ ("International System of Measurement"), commonly known as the "metric system."

Preface

This study was conducted for Headquarters, U.S. Army Corps of Engineers (USACE) under RDTE project 4A162784AT41, "Military Facilities Engineering Technology"; Work Unit AT41-CFM-A001, "Seismic Rehabilitation of Roof and Floor Systems." The technical monitor was Peter Rossbach, CECW-EI.

The work was performed by the Materials and Structures Branch (CF-M) of the Facilities Division (CF), Construction Engineering Research Laboratory (CERL). The CERL Principal Investigator was Steven C. Sweeney. This work was done in cooperation with the Mid-America Earthquake (MAE) Center, headquartered at the University of Illinois, Urbana. MAE Center participants were Dr. Daniel P. Abrams at the University of Illinois and Dr. Roberto Leon at the Georgia Institute of Technology, Atlanta. Some of the work reported here was previously published as a Master's Thesis, "Tri-Directional Seismic Response of Unreinforced Masonry Building Systems" (Orton 2002). The technical editor was Linda L. Wheatley, Information Technology Laboratory – Champaign. Martin J. Savoie is Chief, CF-M, and L. Michael Golish is Chief, CF. The Technical Director of the Facilities Acquisition and Revitalization business area is Dr. Paul A. Howdyshell, CV-ZT, and the Director of CERL is Dr. Alan W. Moore.

CERL is an element of the U.S. Army Engineer Research and Development Center (ERDC), U.S. Army Corps of Engineers. The Commander and Executive Director of ERDC is COL James R. Rowan, EN, and the Director of ERDC is Dr. James R. Houston.

1 Introduction

Background

Unreinforced masonry (URM) is one of the oldest types of building construction and is common throughout the United States. Many masonry buildings were constructed before the development of modern seismic codes and, as a result, some may be susceptible to damage caused by earthquakes and could benefit from seismic mitigation through modification of their structural elements. To design the best seismic retrofit strategy, a clear understanding of the behavior of URM buildings under tri-directional loads must be reached.

Research has already been conducted in the areas of seismic performance of masonry buildings and tri-directional combinations of seismic motions. The research presented in this report is designed to fill in gaps in current knowledge.

Studies in Seismic URM Performance

In 1996, Costley and Abrams published a report on the dynamic response of URM buildings with flexible diaphragms. They studied the response of a half-scale rectangular URM building subjected to uniaxial earthquake loads. Although a great deal of information was learned from this study, they expressed the need for further research to test buildings with an unsymmetrical layout and various pier aspect ratios.

Cohen conducted a study in 2000 on seismic response of low-rise masonry buildings with flexible roof diaphragms. The study focused on the response of floor diaphragms in rectangular half-scale reinforced masonry buildings. He concluded that the building responds as a single degree of freedom system associated with the degree of freedom of the diaphragm.

Tena-Colunga studied the response of a masonry firehouse to the Loma Prieta earthquake. He compared the measured response of the building to several analytical models and found that 3D quasi-dynamic analysis can produce reliable results.

Simsir et al. (2001) studied the influence of diaphragm flexibility on the out-of-plane response of URM walls. Their experiments consisted of uniaxial tests on two out-of-plane URM walls unconnected to two in-plane walls. They found that increased diaphragm flexibility significantly increased the out-of-plane displacement of the URM walls. The increase in displacement was consistent with the increase in period associated with the flexibility of the diaphragm. They also found that the intensity of the axial load affects the out-of-plane demands. Their study, however, did not examine the effect of connecting the out-of-plane walls to the in-plane walls.

The Erbay and Abrams (2001) study on the effect of rehabilitating individual pier samples provides useful information on how rehabilitation influences a single pier; however, individual pier tests do not provide a clear picture of how the rehabilitation will affect the overall building system. Since the interactions between various structural components are largely unknown, the testing of an entire building system is necessary to determine the effectiveness of the retrofit.

Studies in Tri-directional Combinations of Seismic Motions

In 1981 Wilson et al. questioned the acceptability of the square root sum of squares (SRSS) method for combining modal maxima in three-dimensional (3D) analysis. They found that, for torsionally sensitive buildings with modal vibration frequencies that were close, the SRSS method could overestimate the response by as much as 14 times. They presented the complete quadratic combination (CQC) method, which takes into account statistical coupling between closely spaced modes.

Anastassiadis et al. (2002) studied the most unfavorable combination of three simultaneous internal forces. They concluded that, in order to avoid unnecessary overdimensioning, the internal forces could be designed by using the extreme value of one force and the probable values of the others. The extreme and probable values are based on the most critical orientation of seismic excitation. However, their study mainly focused on column behavior where the internal forces in question were the x and y bending moments and the axial force. They did not consider behavior of a masonry pier, for which lateral strength is highly dependent on axial stress.

Lopez et al. (2001) evaluated combination rules for multicomponent seismic analysis. They found that the current combination rules of SRSS, 30 percent, and 40 percent produced errors as large as 18 percent in estimating the design forces to be used. They also concluded that the critical response increases when the vibration periods of the two modes most associated with the orthogonal

directions of horizontal ground motion become close to each other. However, their study did not include systems for which orthogonal lateral force resisting systems were not independent, such as in masonry buildings.

Hwang and Hsu (2000) conducted an experimental study examining base isolated buildings under triaxial ground excitations. They studied a series of symmetrical and unsymmetrical base isolated buildings under independently and simultaneously applied ground motions. They found that vertical accelerations may dramatically increase maximum story accelerations for cases where there is eccentricity on the isolation system. They also found that the maximum displacement predicted from the 100 percent–30 percent combination rule might not be conservative.

Objectives

The objectives of the project focus on achieving a better understanding of the seismic response of URM buildings. Specific objectives include:

- Investigate the effect of tri-directional base motions on the test model.
- Examine dynamic amplification in systems with flexible diaphragms.
- Verify the extrapolation of individual component behavior to the overall response of the building system.
- Provide fundamental knowledge needed to develop seismic protection design.

Approach

This report presents work done jointly between the University of Illinois, the Mid-America Earthquake Center, and the U.S. Army Engineer Research and Development Center (ERDC) Construction Engineering Research Laboratory (CERL). Prototypical structures and gaps in current knowledge were evaluated to determine the characteristic structural features of the test specimen. Preliminary analysis was performed to ensure the desired structural behavior was present. Special attention was paid to the actual material properties of the test specimen and the effect of scaling on it.

To analyze the seismic response of URM buildings, a test model was used that contains important features common to URM buildings such as perforated shear walls and flexible diaphragms. Analytical models were developed to estimate the effect of tri-directional seismic motions on the half-scale model. The structural components, namely the masonry piers and wood diaphragms, were analyzed. The complete building system was analyzed using equivalent static,

response spectrum, linear time history, and pushover analysis. Each analysis method included careful consideration of the directions of load application. Seismic loads were applied independently along each coordinate axis and simultaneously along all three directions.

In this report, the building's response to an independently applied component is compared to simultaneously applied components, and critical combinations are identified. In addition, the design methods suggested by building codes are evaluated considering the actual behavior of the model. Finally, conclusions and recommendations for further research are presented.

Scope

The analytical study presented here is part of an overall project that includes a half-scale dynamic test of the test model, and a study of rehabilitation methods on that model. It works in parallel with a full-scale static test being performed at the Georgia Institute of Technology. The same prototype was developed for the full-scale static and half-scale dynamic tests in order to increase the relevance of the results.

Mode of Technology Transfer

The information presented in this technical report will be presented to U.S. Army Corps of Engineers (USACE) through USACE Structural Engineering Workshops and at professional technical conferences. The results of this study shall be used to evaluate the behavior of a model building tested as part of the overall scope of the research project. Information developed in this project will be submitted for incorporation into FEMA and model building code documents for the seismic design, evaluation, and mitigation of structures. This report will be made accessible through the World Wide Web (WWW) at URL: http://www.cecer.army.mil

2 Description of Test Structure

The test structure described in this section was designed to be used in a triaxial dynamic test. This report presents the analytical study of the half-scale test structure; therefore, all models and calculations are based on the actual design.

Prototype Development

The prototype for the test structure was developed as part of a collaborative effort between the University of Illinois and the Georgia Institute of Technology. The prototypical structure was designed to be representative of older unreinforced brick buildings, such as the firehouse in Figure 2-1. The test structure is two stories to represent a common low-rise URM building. One wall (with an identical in-plane wall) represents a typical masonry wall with windows and doors, as would be found in a masonry house or military barracks. Another wall represents a firehouse garage with a large opening, but is also similar to a storefront. The final wall is nearly solid; typical of a sidewall or back wall to a store. The diaphragms at both the second floor and roof levels are wood floor decking (Figure 2-2).

Figure 2-1. St. Louis firehouse.

The test structure was also designed to reveal behavioral tendencies that meet the objectives of the overall project. The window walls were designed to study the effects of rehabilitating a selective pier on the overall performance of the structure. The two central piers in each wall increase the number of piers for selective retrofit. The walls are identical in configuration in order to provide uniformity and consistency in the structure. The solid and open walls create a torsional irregularity that is common to many masonry buildings. They are also designed to examine the effects of rehabilitating a weak wall that works in parallel with a strong wall. The flexible diaphragms will deliver the same horizontal load to each wall, independent of the walls' relative strengths or stiffness; therefore, effects of strengthening the weak wall on system performance are accentuated. Finally, these types of wall/pier combinations are also typical of actual construction and will help determine the response of real buildings to earthquakes.

Inherent inadequacies exist in both full-scale static tests and half-scale dynamic tests. Individual full-scale static tests do not accurately represent strain rate effects or true inertial force distributions. On the other hand, individual reduced-scale dynamic tests are often disregarded due to their reduced size and use of simulated material. The goal here was to design prototype structures with similar design and expected behavior such that, when both tests are done in parallel, the results become more significant. The analysis done for this report will add to the relevance of the results.

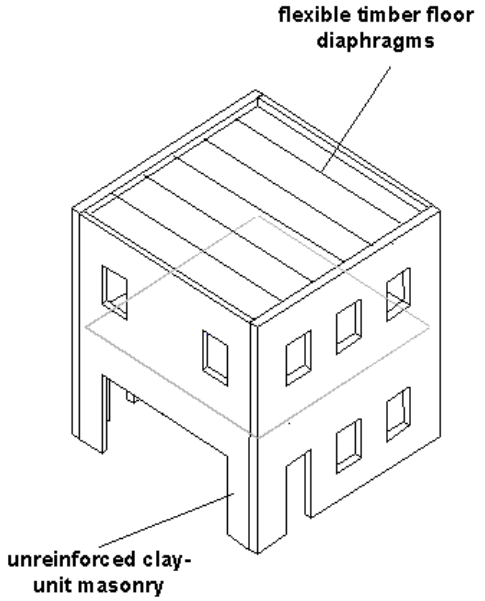

Figure 2-2. Prototype of test structure.

Masonry Design

With the basic design for a prototype developed, the actual layout and design details of the test structure were then determined. The elevations for the walls can be seen in Figures 2-3 through 2-5. The size of the shake table determined the outer dimensions of the test structure. The plan of the test structure (Figure 2-6) measures 148 in. by 150 in., which fits by aid of a concrete base girder on the 12 ft by 12 ft shake table.

The dimensions of the windows and doors were selected based on typical construction, available length of the walls, and the dimensions of the bricks. The doors measure 20 in. by 42.8 in., which is comparable to a typical 3 ft by 7 ft door. The windows measure 20 in. by 24.6 in., which is comparable to 3 ft by 4 ft window. The windows were made 20-in. wide in order to fit two central 20-in. wide piers in walls A and B.

Walls A and B are three wythes thick to be representative of typical bearing walls. Walls 1 and 2 are two wythes thick to be representative of typical non-load bearing walls. Each wall is constructed with a header course every six rows. The mortar is type O (1:2:9) to represent weak mortar typically found in older buildings.

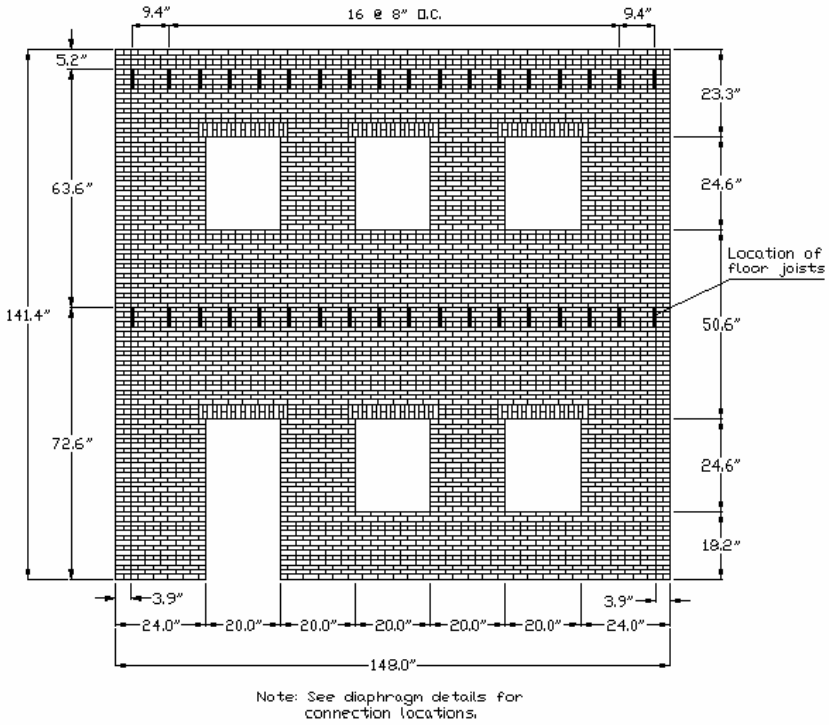

Figure 2-3. Elevation of walls B and A (reverse).

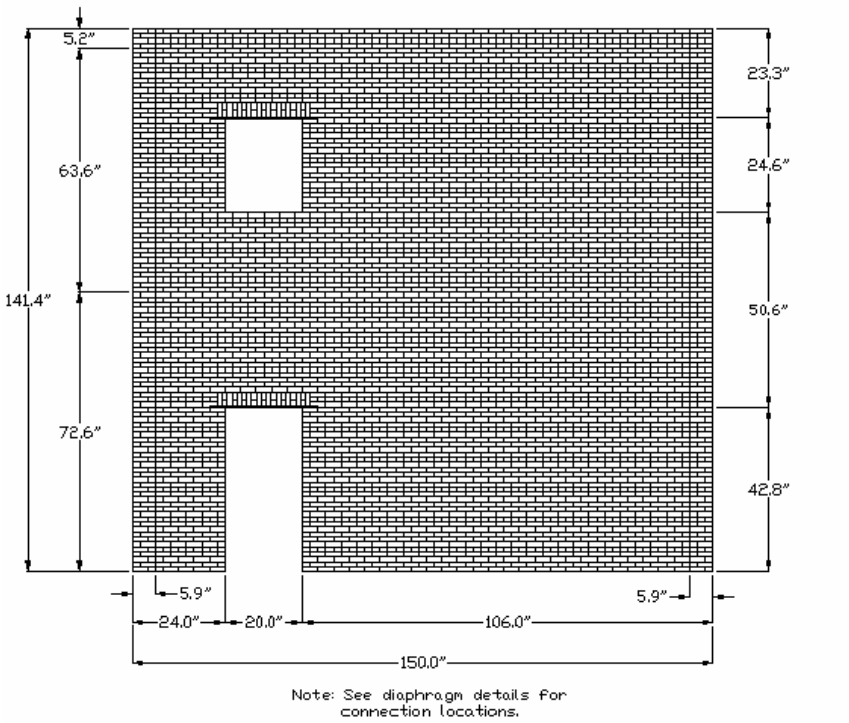

Figure 2-4. Elevation of wall 1.

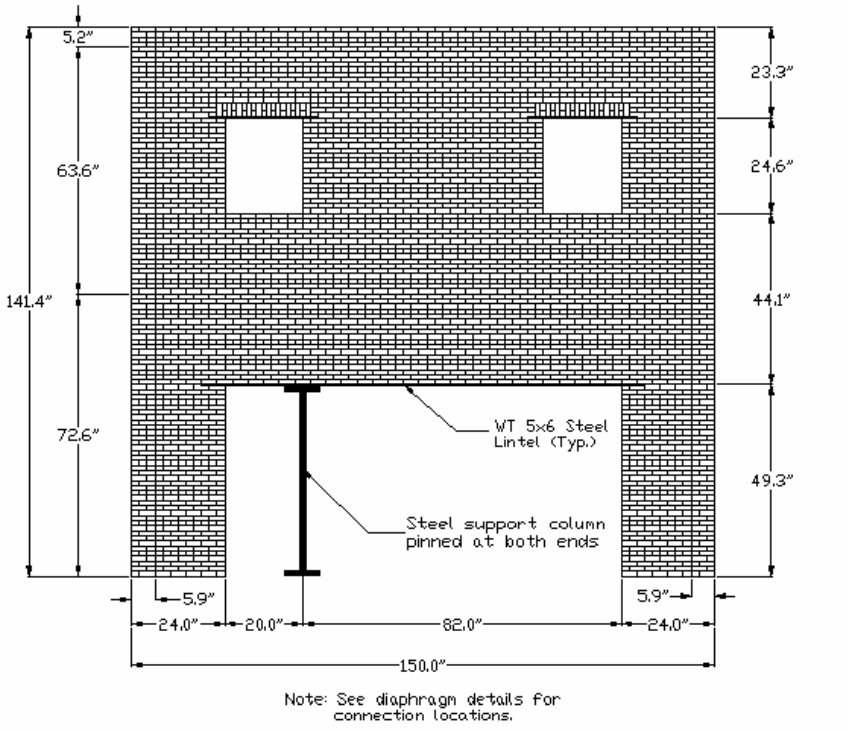

Figure 2-5. Elevation of wall 2.

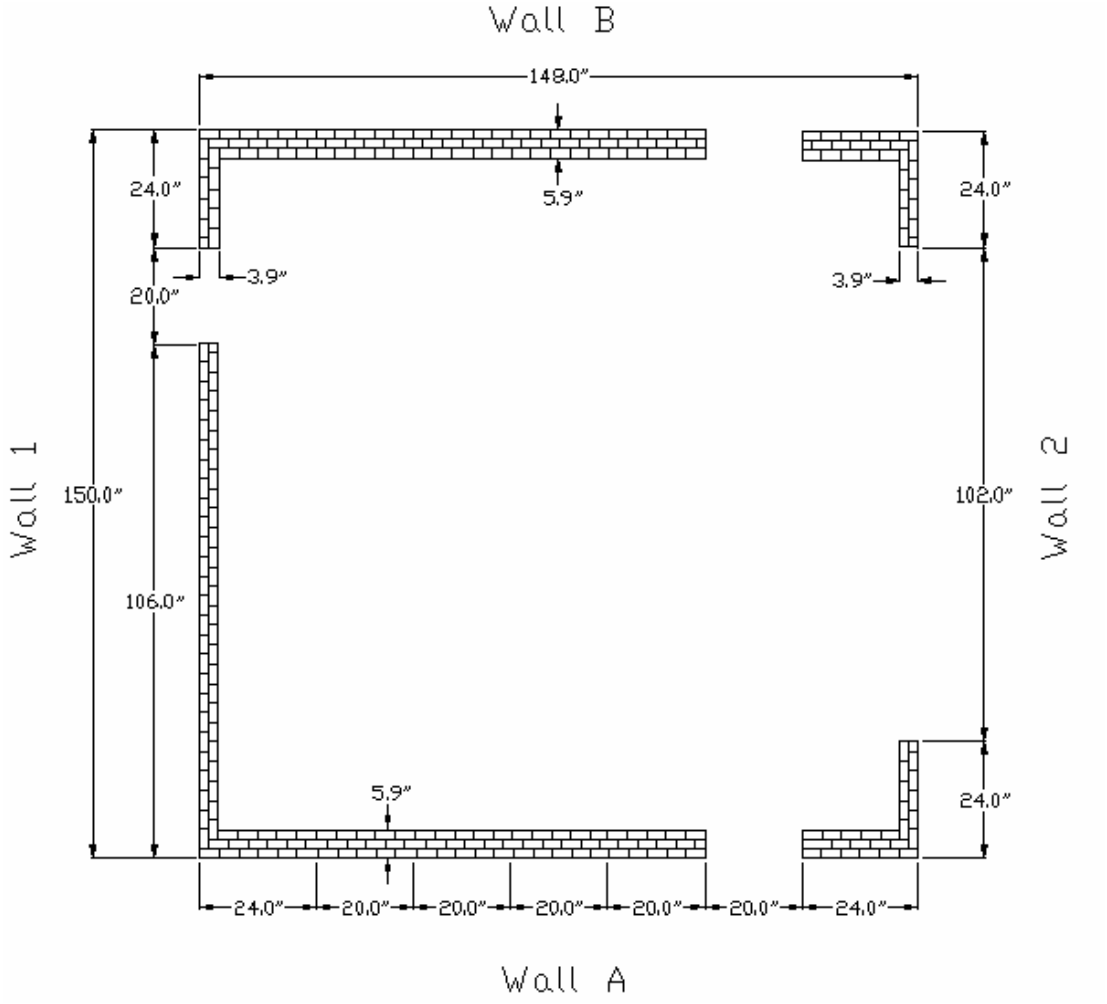

Figure 2-6. Plan of test structure.

Wall 2 was designed to be typical of a wall with a large garage door and an adjacent standard door. The brick pier that would typically exist between them would likely sustain severe damage during testing, and could potentially be dangerous. Therefore, a steel column was added to simulate the behavior of a brick pier without failing during testing. The support column was pinned at both ends by use of two plates with a steel ball in the center, as seen in Figure 2-7. This allowed the support column to move freely in all directions, while providing vertical resistance. A similar type of construction is used in existing buildings, where a steel column is located behind the brick pier.

Figure 2-7. Pin connection for steel support column.

The large opening on wall 2 required the use of a steel lintel. To limit the deflection to the l/600 maximum prescribed by the Masonry Standard Joint Committee (MSJC 1999), a steel WT5x6 was used. The lintel is continuous over the steel support column. The other lintels in walls 1 and 2 are also WT5x6 sections. URM lintels were designed for walls A and B.

The test specimen was constructed between August and December 2001. The test structure was constructed off of the shake table and then lifted onto the table by aid of a concrete base girder. Figure 2-8 shows two professional masons constructing the walls at the CERL test facility. Figure 2-9 shows the completed structure.

Figure 2-8. Construction of test specimen.

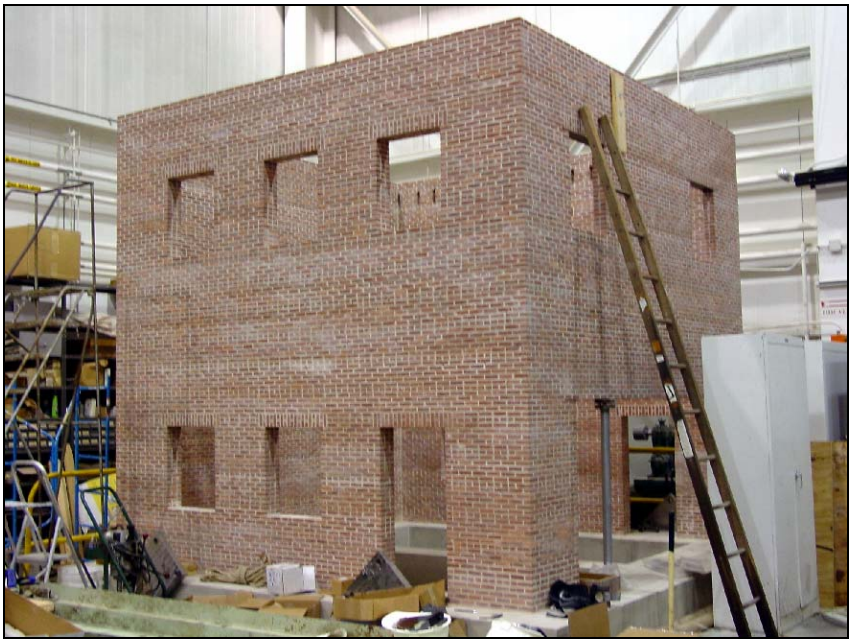

Figure 2-9. Completed test structure.

Diaphragm Design

The floor and roof were designed as typical wood diaphragms. The design is identical for both floors and consists of ¼-in. diagonal sheathing and 1x5-in. joists, shown in Figure 2-10. The diaphragm is tied to each wall by ¼-in. threaded steel bars. The details of the joist-to-wall connections along walls A and B are

illustrated in Figure 2-11, and the locations are shown on the walls in Figure 2-10. Walls 1 and 2 are bolted to the outermost joist on each side of the floor. The diaphragm is designed to obtain frequency ratios between the wall and the diaphragm that realistically emulate prototypes. This design will allow a distinction between the motions of the diaphragms and the walls in the analysis.

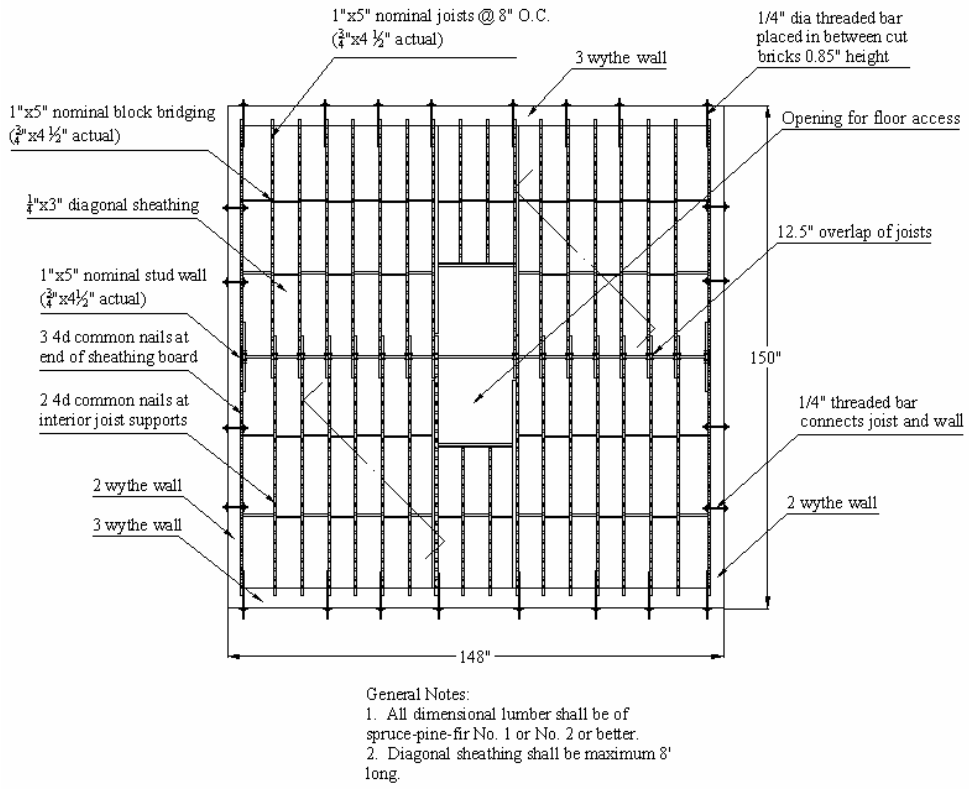

Figure 2-10. Plan of diaphragm.

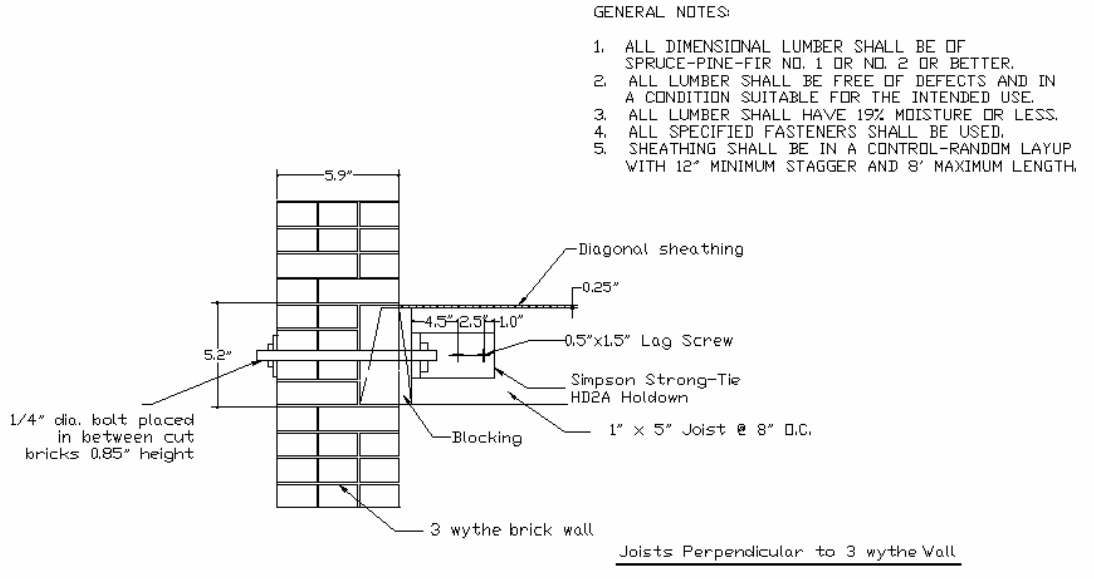

Figure 2-11. Connection detail.

Material Properties

Full-size bricks measuring 7.625 in. x 3.625 in. x 2.125 in. were cut into halves along each axis to make half-scale bricks (Figure 2-12). A circular saw was used to cut the bricks as seen in Figure 2-13. This produced eight half-scale bricks that measure approximately 3.75 in. x 1.75 in. x 1 in., taking into account the 1/8-in. width taken up by the saw blade. The bricks used in this test were common solid clay pavers.

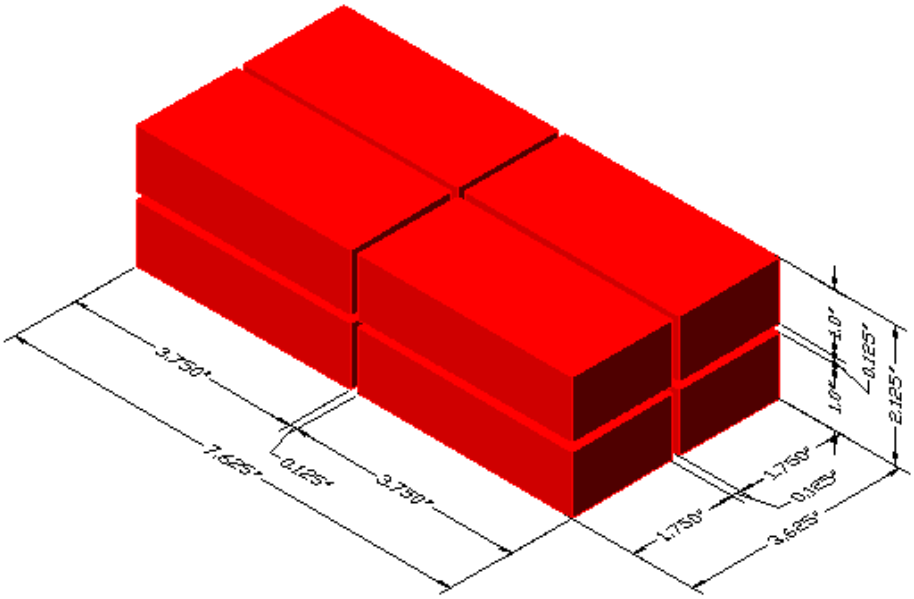

Figure 2-12. Dissection of full-scale brick into half-scale sections.

Figure 2-13. Cutting half-scale bricks.

Ten half-scale bricks were tested to determine their actual size, initial rate of absorption (IRA), modulus of rupture, compressive strength, and modulus of elasticity using American Society for Testing and Materials (ASTM) C 67 – 98a standard tests. Table 2-1 lists the results.

Table 2-1. Results of brick tests

Length	3.73	±	0.02	in.
Width	1.78	±	0.03	in.
Height	1.06	±	0.04	in.
IRA	9.05	±	2.11	g/min/30 $in.^2$
Modulus of Rupture	0.633	±	0.087	ksi
Compressive Strength	15260	±	3145	psi
Modulus of Elasticity	44320	±	1134	ksi

Twenty prisms were built during the construction phase of the model. The prisms were tested using ASTM standard tests for flexural bond strength (E 518 – 00a), masonry bond strength (C1357 – 98a), and compressive strength (C 1314 – 98a). Table 2-2 gives the results of the tests. In addition to the prism tests, ten mortar cubes were tested in accordance with ASTM standards. Pictures from the material tests are shown in Figures 2-14 through 2-18.

Table 2-2. Results of prism and mortar tests

Prism Compressive Strength	4.58 ± 0.56	ksi
Prism Elastic Modulus	527.13 ± 228.42	ksi
Mortar Compressive Strength	172.59 ± 81.69	psi
Mortar Elastic Modulus	23.78 ± 12.78	ksi
Prism Tensile Strength	79.09 ± 12.59	psi
Prism Flexural Bond Strength	91.72 ± 39.41	psi

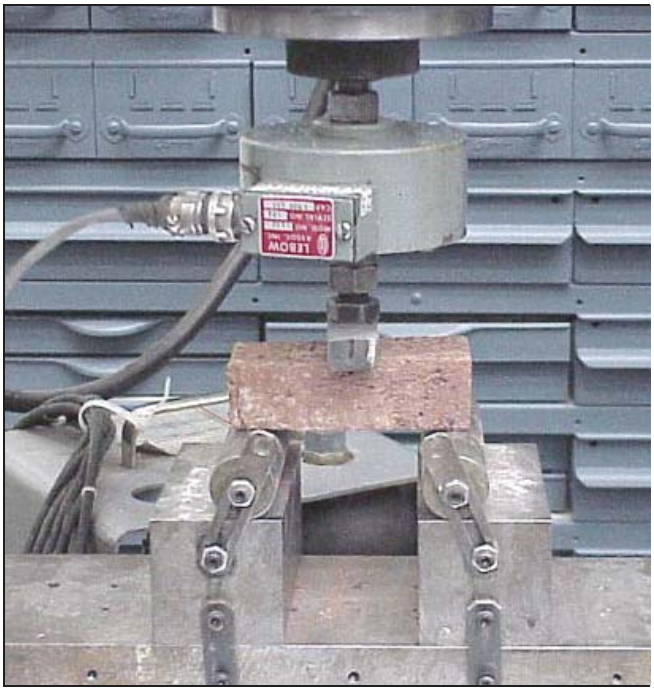

Figure 2-14. Modulus of rupture test of individual brick.

Figure 2-15. Compression test of prism.

Figure 2-16. Compression test of mortar cube.

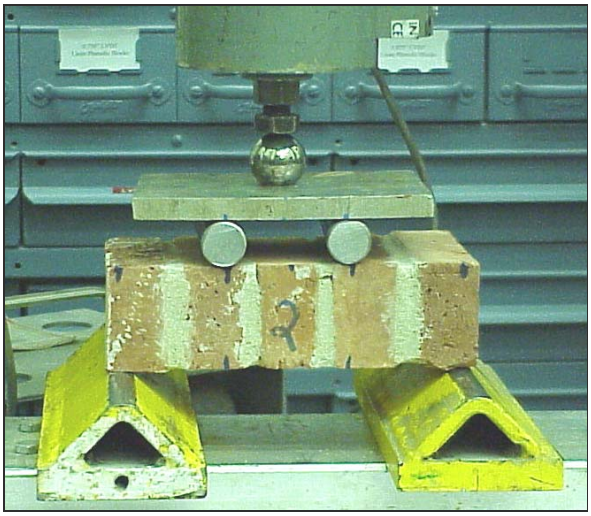

Figure 2-17. Flexure test of prism.

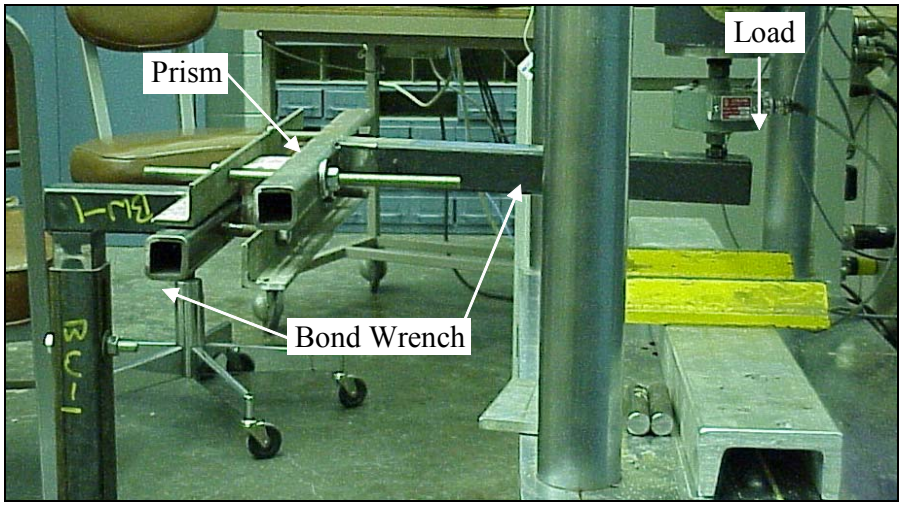

Figure 2-18. Bond wrench test of prism.

Scaling

A common problem in reduced-scale testing is that, in creating a model, not all of the properties can be scaled. As an example, the half-scale test structure was constructed using half-scale bricks; however, the bricks possess the same material properties (elastic modulus and density) as the full-scale bricks.

The scaling relationships inherent to the model are presented in Equation 2-1. When these relationships are applied to accurately scale the gravity stress, Eq 2-2 results. Consequently, the gravity stress versus the material strength relationship is not constant if the densities of the two materials are the same (Harris and Sabnis 1999). This relationship is important for masonry construction because the lateral strength of the piers is based, in part, on vertical stress.

$$l_{model} = \frac{1}{2} l_{prototype} \qquad E_{model} = E_{prototype} \qquad \text{Eq 2-1}$$

$$\left(\frac{\gamma l}{E}\right)_{model} = \left(\frac{\gamma l}{E}\right)_{prototype} \qquad \gamma_{model} = 2\gamma_{prototype} \qquad \text{Eq 2-2}$$

The density of the bricks is half what it should be for a true-scale model; therefore, in order to effectively double the density of the brick, additional weight should be added throughout the volume of the walls. Unfortunately, adding distributed mass is not feasible; therefore, weight was added in a disperse pattern on the wall faces.

To double the density, 21,200 lb of extra weight was added to the test structure. Some of the weight was added to the perimeter of the floor diaphragms in order to accentuate their dynamic response, and the remainder was bolted to the walls. The final plan was to bolt ~60-lb lead weights to the walls in a disperse pattern that would not interfere with the cracking behavior of the piers. This plan resulted in weights concentrated around the spandrels of the test structure as shown in Figure 2-19.

Additional weight concentrated around the spandrels rather than throughout the volume of the walls does not pose a serious analytical concern. This type of model is accurate while the material is in the elastic range; therefore, the crack patterns will still be similar. In the inelastic range, the modeling of gravity stress does affect the accuracy of the model. However, the point of the overall project is to study the global response characteristics and to evaluate the retrofit measures. Since the model will show similar crack patterns, the response of the cracked model will contain the same global characteristics as the full-scale model.

To model the test structure using finite element analysis programs, the density of the material was simply doubled. Furthermore, the time scale of the earthquake motions was divided by the square root of 2. This division is supported by the scaling relationships presented in Equations 2-3 and 2-4.

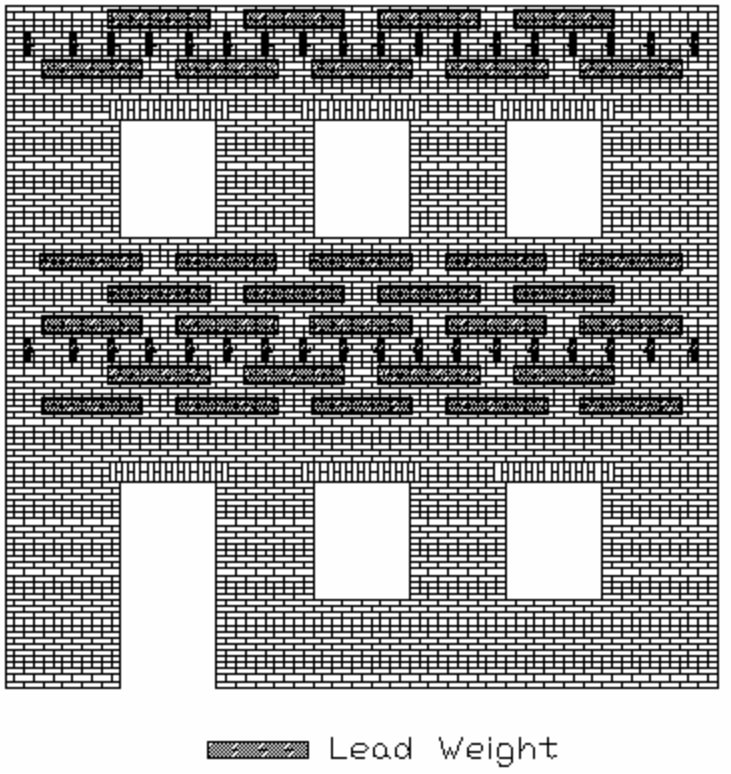

Figure 2-19. Layout of additional weight.

$$\frac{f_{model}}{f_{prototype}} = \frac{\left(\sqrt{K/M}\right)_{model}}{\left(\sqrt{K/M}\right)_{prototype}} = \frac{\left(\sqrt{\frac{EI^2/l}{\gamma l^3}}\right)_{model}}{\left(\sqrt{\frac{EI^2/l}{\gamma l^3}}\right)_{prototype}} = \sqrt{2} \qquad \text{Eq 2-3}$$

$$f = 1/T \qquad \frac{T_{model}}{T_{prototype}} = 1/\sqrt{2} \qquad \text{Eq 2-4}$$

With these scale factors determined, Table 2-3 can be constructed to represent the model/prototype scale factor for various quantities.

Table 2-3. Scaling relationships.

Quantity	Scale Factor (S_m/S_p)
Force	1/4
Stress	1
Acceleration	1
Velocity	1/√2
Time	1/√2
Frequency	√2
Length	1/2
Displacement	1/2
Modulus	1
Strain	1
Density	2

Base Girder

The test structure was mortared to a concrete base girder, which was designed to support the model as it was moved onto the shake table. During testing, it remained stiff and acted as a rigid connection between the table and the building. The base girder (seen in Figure 2-20) has perimeter beams that are 1-ft thick and 2-ft 3-in. wide, with an additional interior beam of the same thickness and a 1-ft width. It consists of reinforced concrete that is post-tensioned to provide additional strength during lifting of the test structure onto the shake table. The base girder is bolted to the shake table with 25 1½-in. bolts.

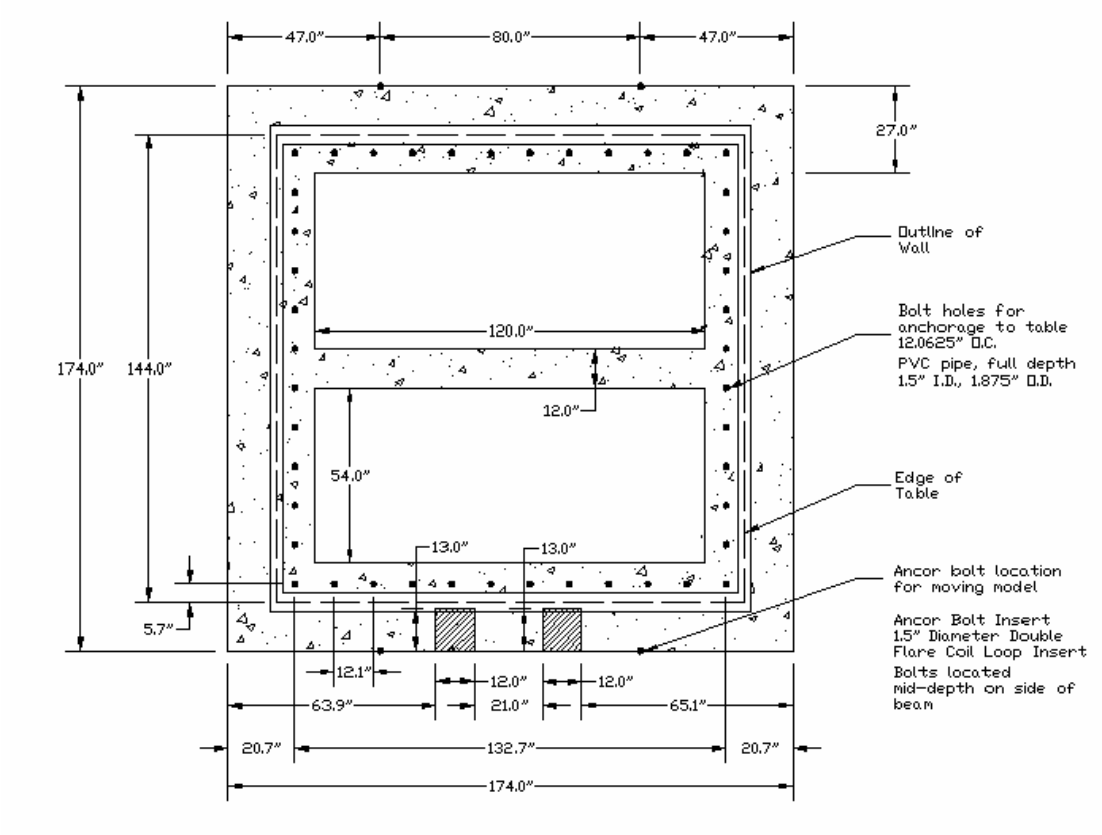

Figure 2-20. Layout of base girder.

3 Component Analysis

The behavior of a building system derives, in part, from the behavior of the components of that system. A clear understanding of component behavior will help to determine the tri-directional effects of seismic motions on the building system. For the test structure under consideration, this includes the behavior of the masonry and timber materials, as well as the behavior of various subassemblages, such as the piers and the diaphragms.

Masonry Behavior

The behavior of masonry buildings derives from its inherent material properties, and the behavior of masonry subassemblages.

Masonry Material Behavior

In its simplest form, masonry consists of bricks (in this case, clay bricks) joined together by mortar. The bricks and mortar have their own unique properties that produce an inhomogeneous conglomeration when combined during construction. Part of the inhomogeneity exists because the masonry is assembled piece by piece and, as a result, there is no way to ensure that every brick is placed in exactly the same way as the brick before it. Moreover, the bricks and batches of mortar will likely have varying properties. The main characteristics of masonry behavior can be summarized as follows (Beskos and Anagnostopoulos 1997):

- Mechanical behavior is inhomogeneous,
- Masonry is not isotropic,
- Tensile resistance is close to zero,
- Compressive resistance is fragile (no yielding),
- Mechanical behavior is not linear and not elastic.

This level of complication requires some simplifying assumptions for analysis. One assumption typically adopted is that masonry is isotropic and homogeneous. In addition, at small stress levels, masonry can be assumed to be linear-elastic.

Independent Pier Behavior

An important part of seismic analysis of a masonry structural system is determining the lateral behavior of the constituent piers. Piers are the structural elements of a masonry wall and are designed to carry the demands of both vertical and lateral loads. They can generally be identified as the continuous portions of a wall located on either side of openings such as windows or doors. Consequently, there can be many piers in a perforated shear wall, but a solid wall, having no openings, behaves as a single pier (see Figure 3-1). The response of the piers can be combined to help determine the behavior of an individual wall or the entire building.

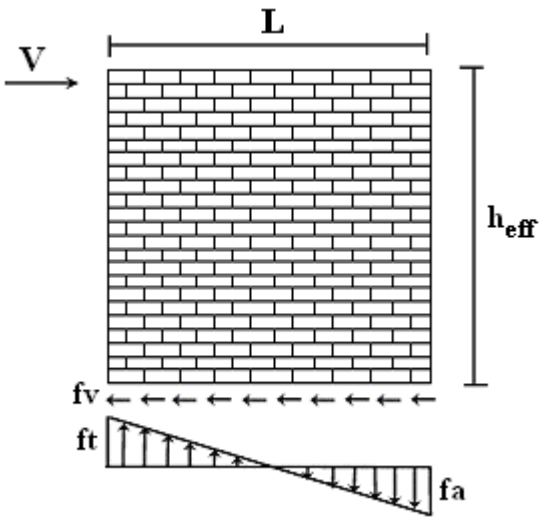

Figure 3-1. Forces on free-standing pier.

The Federal Emergency Management Agency's (FEMA's) "Prestandard and Commentary for the Seismic Rehabilitation of Buildings," FEMA 356, provides a straightforward method to determine the lateral force-deformation relationship of masonry piers. The prestandard is a prescriptive method similar to most building codes and is comparable to what is used in practice. FEMA 356 was used during the design phase of this project to ensure that the desired structural response would be present.

The lateral behavior of a masonry pier prior to yielding is linear-elastic, and can be identified as the initial straight-line portion of the load-deflection curve (see Figure 3-6, p 29). At the onset of yield, a failure mechanism occurs, causing increased deflections and loss of resistance. The slope of the load-deflection curve in the linear-elastic region is the elastic stiffness of the pier. FEMA 356 presents two formulations to calculate the stiffness of a pier; the first for cantilevered walls and the second for piers that have full restraint against rotation at the top

and bottom. They are presented below as Equation 3-1 and Equation 3-2, respectively.

$$k_{pier} = \frac{1}{\frac{h_{eff}^{3}}{3E_m I_g} + \frac{h_{eff}}{A_v G_m}} \quad \text{Eq 3-1}$$

$$k_{pier} = \frac{1}{\frac{h_{eff}^{3}}{12E_m I_g} + \frac{h_{eff}}{A_v G_m}} \quad \text{Eq 3-2}$$

where h_{eff} is the pier height to the point of lateral load, E_m is the masonry elastic modulus, A_v is the effective shear area (assumed to be 5/6 of the gross area), I_g is the moment of inertia of the uncracked pier cross section, and G_m is the shear modulus (assumed to be 0.4 E_m). The values for stiffness of the piers are presented in Table 3-2.

The lateral strength of piers in URM walls depends on the mode of failure. FEMA 356 recognizes four different types of failure: bed-joint sliding, rocking, diagonal tension, and toe crushing. The strength calculations for each mode are presented below and are also given as Equations 7-3 through 7-6 in the FEMA document.

Bed-joint sliding failure occurs when the shear stress along the base of the pier (fv in Figure 3-1) is greater than the shear strength of the pier. When the shear strength is reached, a crack forms along the length of the bed joint and the pier begins to slide. The bed-joint sliding strength, V_{bjs}, is given below as Equation 3-3, where v_{me} is the bed-joint sliding shear strength and A_n is the net area of the mortared section.

$$V_{bjs} = v_{me} A_n \quad \text{Eq 3-3}$$

The rocking mode of failure occurs when a crack forms at the bottom of the pier (top and bottom for a fixed-fixed case), allowing it to rock laterally. The crack forms when the tensile stress (ft in Figure 3-1) becomes greater than the axial load stress (f_a) plus tensile strength of the masonry (f_t). This occurs when the lateral load is:

$$V_{crack} = \frac{L^2 t}{6h}(f_a + f_t) \quad \text{Eq 3-4}$$

This equation is specifically for a cantilevered pier, as shown in Figure 3-1. For a fixed-fixed pier, multiply Equation 3-4 by two. Once cracks have sufficiently formed over the length of the pier, the rocking strength is reached (Equation 3-5). The formula for determining rocking strength is a function of the expected axial compressive force (P_E), the ratio of the pier length (L) to the effective height of the pier (h_{eff}), and a factor α equal to 0.5 for a fixed-free cantilevered wall and 1.0 for a fixed-fixed pier.

$$V_r = 0.9\alpha P_E\left(\frac{L}{h_{eff}}\right) \quad \text{Eq 3-5}$$

Diagonal tension failure is characterized by X cracks through the wall or pier caused by internal stresses. If the cracks pass through the mortar in a stairstep pattern, the strength of the pier is the same as the bed-joint sliding strength of Equation 3-3. However, if the cracks propagate diagonally through the mortar and the bricks, the strength is given by Equation 3-6:

$$V_{dt} = f'_{dt}\, A_n\left(\frac{L}{h_{eff}}\right)\sqrt{1+\frac{f_a}{f'_{dt}}} \quad \text{Eq 3-6}$$

where f'_{dt} is the lower bound masonry diagonal tension strength and f_a is the lower bound axial compressive stress.

Toe crushing is the failure of the bricks and mortar at the corners of the pier due to the additional compressive stresses of the overturning moment (fa in Figure 3-1). Toe crushing strength is determined using Equation 3-7:

$$V_{tc} = \alpha P_L\left(\frac{L}{h_{eff}}\right)\left(1-\frac{f_a}{0.7f'_m}\right) \quad \text{Eq 3-7}$$

where f'_m is the lower bound masonry compressive strength and the ratio of L/h_{eff} shall not be taken less than 0.67.

The FEMA 356 equations were used to determine the lateral strength of the piers in the test structure. The results are presented in Table 3-1, with pier numbers shown in Figure 3-2 (piers 1-4 are associated with wall A). For these calculations, v_{me} was assumed to be 35.1 psi and f'_{dt} to be 27 psi in accordance with the default properties in Section 7.3.2.10 of FEMA 356. Furthermore, f'_m was calculated to be 2,862 psi by taking the prism compression strength

presented in Chapter 2 and dividing by 1.6, as prescribed by Section 7.4.2.2.2 of FEMA 356. The remainder of the pier properties used in the strength equations were calculated based on the actual dimensions of the test structure and the weight of the structure equal to 20 psf per wythe.

Table 3-1. Pier lateral strengths based on FEMA 356

Pier (wall)	L (in.)	h_{eff} (in.)	V_{bjs} (kip)	V_r (kip)	V_{dt} (kip)	V_{tc} (kip)
1 (A)	24	24.6	4.89	3.11	5.12	3.41
2 (A)	20	24.6	4.08	2.16	3.55	2.37
3 (A)	20	24.6	4.08	2.16	3.55	2.37
4 (A)	24	42.8	4.89	1.83	2.96	2.40
5 (B)	24	24.6	4.89	3.11	5.12	3.41
6 (B)	20	24.6	4.08	2.16	3.55	2.37
7 (B)	20	24.6	4.08	2.16	3.55	2.37
8 (B)	24	42.8	4.89	1.83	2.96	2.40
9 (1)	106	141.4	14.51	2.51	10.81	2.77
10 (1)	24	42.8	3.29	0.78	1.80	1.03
11 (2)	24	49.3	3.29	1.65	1.94	2.47
12 (2)	24	49.3	3.29	1.65	1.94	2.47

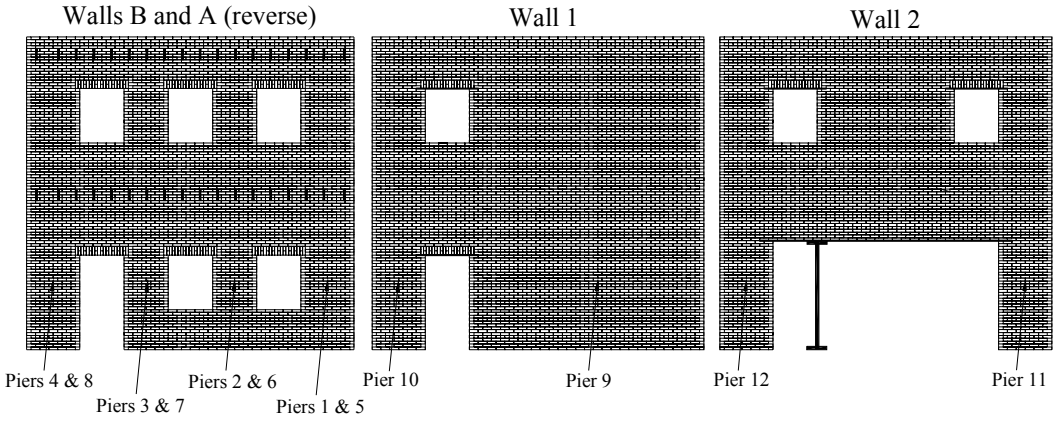

Figure 3-2. Pier numbers.

The results of the analysis indicate that all of the first story piers should fail by rocking, although the toe crushing strengths are only slightly larger. The second story pier strengths are not reported because they will not receive enough inertial force to cause damage. As a result, the building is essentially rigid above the first story piers.

Table 3-1 presents pier strengths that were calculated assuming that the compressive stresses in the piers were due only to gravity loads. When a wall is loaded laterally, however, overturning moments will cause increased compressive stresses on one side of the wall and decreased stresses on the other side. Based on the FEMA 356 equations, it is clear that the lateral strength of a pier

is greatly dependent upon compressive stress; however, the degree of dependency varies for different failure types. As a result, if the compressive stress in a pier is increased or decreased by a sufficient amount, the mode of failure for the pier can change. An example of this variation is illustrated in Figure 3-3 for piers with L/h_{eff} equal to 0.81 (piers 2, 3, 6, and 7). As seen in the figure, the mode of failure will change from rocking to bed-joint sliding when the vertical load reaches 5,600 lb.

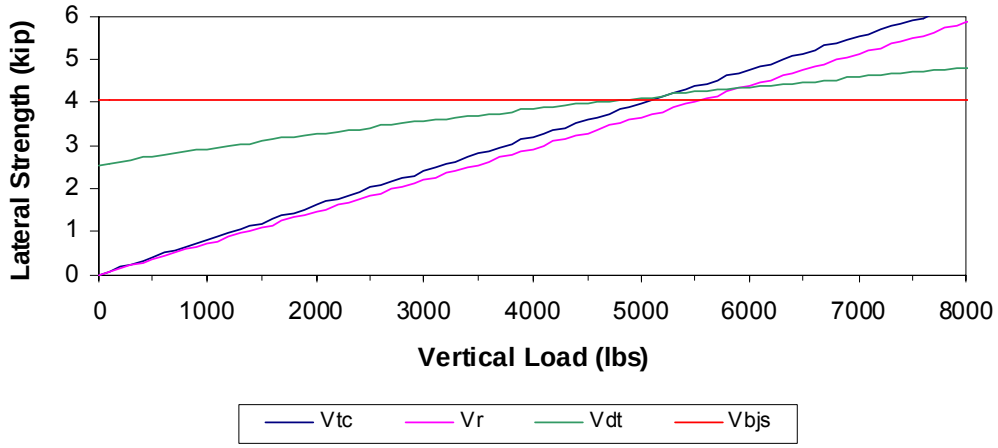

Figure 3-3. Variations of lateral strength based on vertical load of a 20 x 24.6-in. pier based on FEMA 356.

Behavior of Piers in Laterally Loaded Walls

The effect of overturning moment on the overall strength of a wall is dependent upon the direction of loading and the relative locations and load-deformation properties of the constituent piers. For example, consider wall A, shown in Figure 3-2. The initial strengths of the piers under gravity load are controlled by rocking behavior and are equal to 1.83, 2.16, 2.16, and 3.11 kips for piers 4, 3, 2, and 1, respectively (moving left to right along the figure). The first case to be examined is for lateral load to be applied at the left side of the wall, pushing the structure to the right. Figure 3-4 is a plot of the lateral strength of the wall versus the applied base shear. There are several important points to make regarding the figure. Comments are made from the point of zero load to failure of the wall:

- The overturning moment resulting from the lateral forces will cause piers 1 and 2 to increase in compressive stress and lateral strength, and piers 3 and 4 to decrease.
- The rate at which pier 1 initially gains strength from increased vertical load (controlled by rocking) is greater than the rate at which pier 4 loses strength

since the ratio of L/h_{eff} is greater for pier 1 (See Equation 3-5 and Table 3-1). As a result, the overall strength of the wall increases.

- Piers 2 and 3 gain/lose vertical load at nearly the same rate and are both controlled by rocking; therefore, their overall strength contribution remains fairly constant at about 4.4 kips.
- The mode of failure for pier 1 changes to bed-joint sliding at a base shear equal to 3.4 kips and, at this point, its lateral strength becomes constant at 4.89 kips. The mode change is consistent with what is shown in Figure 3-3.
- The rocking strength of pier 4 decreases as it is relieved of vertical load until it reaches a zero stress state at a base shear of 6.0 kips. The strength of the wall decreases as the base shear increases from 3.4 to 6.0 kips.
- The wall strength becomes constant after pier 4 completely fails since the combined contribution from piers 2 and 3 is constant and the bed-joint sliding strength of pier 1 is constant.
- At a base shear of 9.3 kips, the shear force in pier 1 has increased to the bed-joint sliding strength and the wall fails. Note that only pier 1 receives enough vertical load from the overturning moment that its failure mode changes. The other piers all maintain rocking behavior.

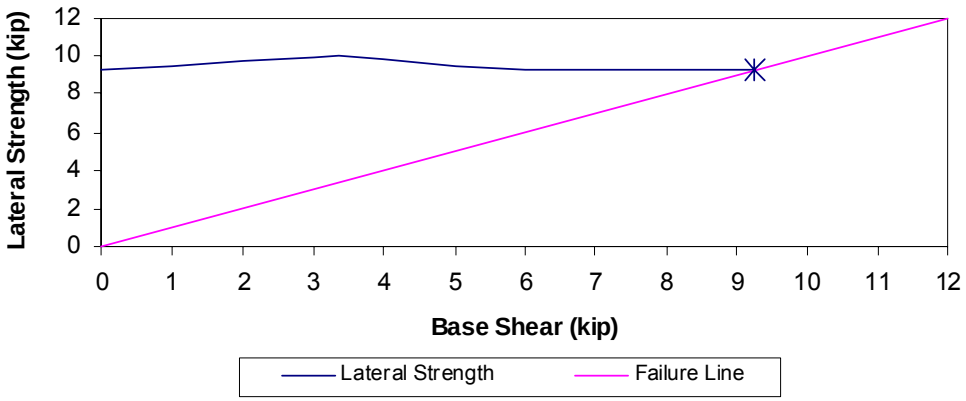

Figure 3-4. Effect of base shear on lateral strength of wall A for loads applied on pier 4 side of wall.

To show the dependency of wall behavior upon the direction of load, Figure 3-5 is a plot of the response of wall A if it is loaded on the right side of the wall. The first important observation is that the strength of the wall initially decreases, because pier 1 is now losing strength more quickly than pier 4 gains strength. A second major difference between the two load cases is that, as the vertical load increases in pier 4, its mode shifts to toe-crushing and not bed-joint sliding. As a result, after pier 1 completely fails at a base shear of 5.4 kips, the wall begins to gain some strength until the toe-crushing strength of pier 4 is reached, resulting

in a brittle failure (Note: Toe crushing strength is not constant with respect to vertical load based on FEMA 356. See Equation 3-7). From the examples presented, it is clear that overturning moment can greatly influence the behavior of a masonry wall, and that the response of the wall must be examined on a case by case basis due to the effects of relative pier properties and load direction.

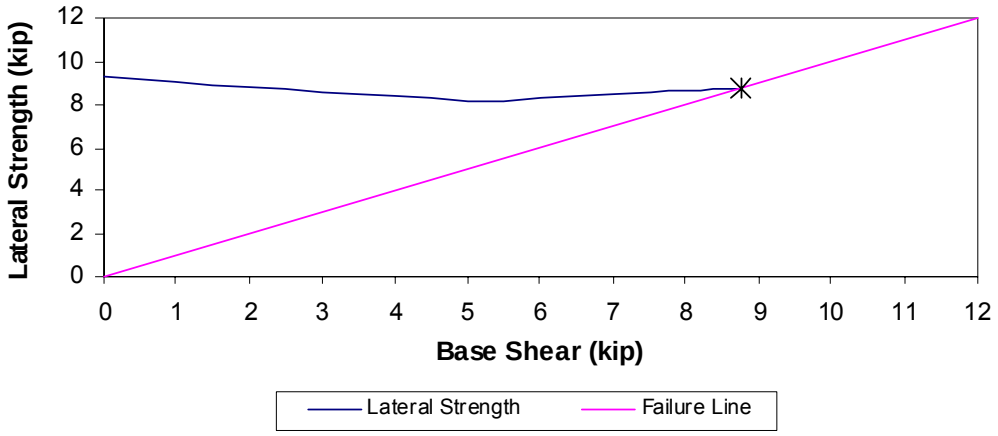

Figure 3-5. Effect of base shear on lateral strength of wall A for loads applied on pier 1 side of wall.

It is important that the reader not confuse Figures 3-4 and 3-5 with a pushover type analysis, since the calculation of the wall strength for a given base shear does not include the reduction of pier strength with increased deflection or the nonlinear effects of large displacements. Instead, the strength was calculated assuming that the structure is at a zero deformation state. Consequently, the figures should be thought of as a way to determine the strength of the wall for an instantly applied base shear, much the way a ground acceleration affects an undamaged building. Pushover analysis is discussed in Chapter 4.

Deformation Response of Piers

Thus far, only the strength of the piers under lateral load has been considered. Of equal importance is the deformation response of the piers, which is shown in Figure 3-6. In the figure, Vy is the minimum strength from Table 3-1, and Δy is determined by dividing Vy by k_{pier} of Equations 3-1 and 3-2, as appropriate. For a given failure mode, FEMA 356 specifies the equations used to determine Δd, Δu, and Vc. For a rocking pier, these values can be computed using Equations 3-8 through 3-10:

$$\Delta d = {0.4\, h_{eff}}^2 \Big/ 100L \qquad \text{Eq 3-8}$$

$$\Delta u = {0.8\, h_{eff}}^2 \Big/ 100L \qquad \text{Eq 3-9}$$

$$Vc = 0.6Vy \qquad \text{Eq 3-10}$$

These equations yield the results for the force deformation relationships in Table 3-2.

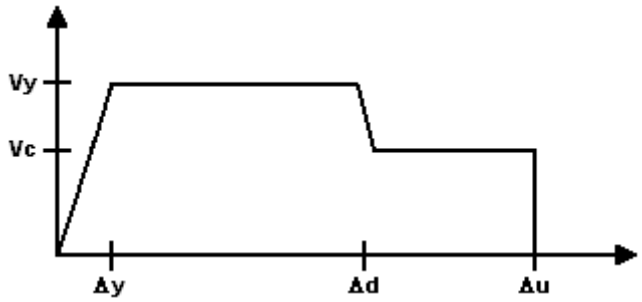

Figure 3-6. Force deformation curve for masonry piers per FEMA 356.

Table 3-2. Pier force deformation behavior

Pier (wall)	k_{pier} (k/in.)	V_{crack} (kip)	V_y (kip)	Δy (in.)	Δd (in.)	V_c (kip)	Δu (in.)
1 (A)	699.68	3.417	3.105	0.00444	0.1009	1.863	0.2017
2 (A)	523.34	2.373	2.156	0.00412	0.1210	1.294	0.2421
3 (A)	523.34	2.373	2.156	0.00412	0.1210	1.294	0.2421
4 (A)	263.58	1.981	1.831	0.00695	0.3053	1.098	0.6106
5 (B)	699.68	3.417	3.105	0.00444	0.1009	1.863	0.2017
6 (B)	523.34	2.373	2.156	0.00412	0.1210	1.294	0.2421
7 (B)	523.34	2.373	2.156	0.00412	0.1210	1.294	0.2421
8 (B)	263.58	1.981	1.831	0.00695	0.3053	1.098	0.6106
9 (1)	144.48	3.513	2.513	0.01740	0.7545	1.508	1.5090
10 (1)	176.93	1.163	0.779	0.00441	0.3053	0.468	0.6106
11 (2)	131.49	1.370	1.648	0.01254	0.4051	0.989	0.8102
12 (2)	131.49	1.370	1.648	0.01254	0.4051	0.989	0.8102

The lateral behavior of individual piers can be combined to determine the lateral behavior of the wall, or the whole building. Such combinations are discussed in the Pushover Analysis section of Chapter 4.

Tri-directional Behavior of Masonry Walls

The previous analysis considered masonry behavior in only one direction, in-plane. For realistic seismic behavior, the out-of-plane and vertical directions must be considered as well. The out-of-plane response of masonry walls is

generally not included in analysis because it is assumed that the walls have little or no strength in that direction. Even though they provide little lateral resistance, out-of-plane wall failures are common (FEMA 306). The out-of-plane response of a masonry wall is generally a rocking behavior about its base, and if it is not adequately restrained by the diaphragm, it may fall out. Even with restraint, however, extensive cracking may allow an unrestrained portion to fail or, if base rotations are large enough, the wall could overturn.

The influence of the connection between the in-plane and out-of-plane walls must also be considered. Most masonry buildings constitute a box system where the connection between the four walls is necessary to resist horizontal action (Beskos and Anagnostopoulos 1997). In this case, the attaching in-plane walls resist load that is directly transferred through the bending of the out-of-plane walls. This is dissimilar to the load path in frame buildings, where no such connection exists between the lateral load resisting systems. As a result, the connection between the perpendicular walls can become highly stressed, often causing a vertical crack to develop. This type of failure is frequently seen in post earthquake investigations (FEMA 306). In addition to damage at the corners of the building, excess axial compression and tension in the connecting flange portions of the out-of-plane walls may result from the global overturning of the building. This change in vertical stress may reduce the lateral strength of the wall's constituent piers.

Another important consideration when performing a tri-directional analysis is determining the severity of torsional effects. Clearly, these effects are of most concern for structures that are irregular; however, even if the building is symmetric, spatial variation in the ground motion may result in a torsional component (Chopra 1995). The twisting motion of the building may contribute additional stresses on the building corners due to the tendency of the rigid perpendicular corner to accommodate angle change. Moreover, the presence of torsion will also affect the base shears in the piers by combining with in-plane shear forces on one side of the building and subtracting on the other side. This effect can be quite large depending on the structure and the ground motion; consequently, the initiation of damage is contingent upon which wall of the building first experiences additive torsional shears.

Vertical accelerations may play an even larger role in damaging a URM building. As seen from the independent pier analysis, the lateral strength of masonry derives in part from vertical stress. When vertical accelerations are applied to the structure, the vertical load will vary and possibly cause increased damage in the building. This damage can be a result of both tensile and compressive inertial forces.

In one case, upward accelerations may decrease the strength of the wall to such a degree that lateral forces far exceed the strength of the wall, resulting in severe damage. As Figure 3-3 indicates, however, increased compressive stress could result in a change in failure mode that is more damaging to the structure. For example, the smaller the vertical compressive stress is in a pier, the more likely it is to rock. Rocking provides a good ductile response, even though it would occur at a lower level of vertical load. On the other hand, as the compressive stress is increased, toe crushing becomes more probable. This failure mode is brittle and potentially very damaging to the building. This vertical sensitivity is another behavior unique to URM buildings.

Diaphragm Behavior

A floor or roof that carries in-plane forces is referred to as a diaphragm. The diaphragm distributes the in-plane forces caused by its own mass and the mass of the out-of-plane walls to the vertical lateral load resisting elements. The distribution of force to the lateral resisting elements (in-plane walls) depends on the characteristics of the diaphragm.

Two basic types of diaphragm behavior are possible depending on the relative rigidity between the diaphragm and the walls. If the deformation of the diaphragm is insignificant compared to that of the walls, it is considered to be rigid. In this case, the diaphragm forces the walls to move together as a unit, thus distributing lateral load in proportion to the walls' stiffness. The second type of diaphragm behavior is the opposite case; the deformation of the walls is insignificant compared to that of the diaphragm. As a result, the walls will resist lateral forces based on the amount of tributary mass they carry, just as a beam would distribute its load between two supports. The wood diaphragms in the test structure are flexible compared to the stiff masonry walls; therefore, each wall will receive in-plane lateral forces proportional to its vertical compressive stress and the demands of the attaching out-of-plane walls.

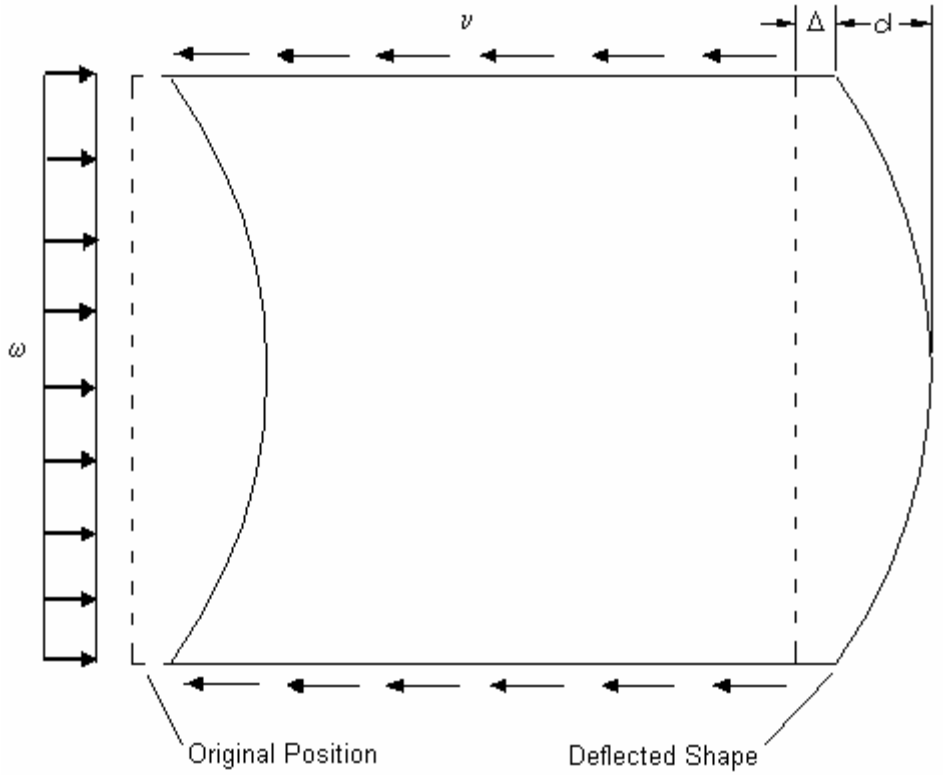

Figure 3-7. Deflection of diaphragm.

In addition to lateral force distribution, the in-plane stiffness of a diaphragm also controls the diaphragm deflection and fundamental frequency, which play important roles in the overall response of a structure. The in-plane stiffness of a wood diaphragm is influenced by the type of sheathing, size and amount of fasteners (nails), and the existence of perimeter chords (FEMA 356). Unfortunately, due to the complex mechanisms that contribute to their flexibility, namely the behavior of the nails, the in-plane stiffness of wood diaphragms cannot be predicted by simple analysis (Cohen 2001). There have been several attempts to come up with a simple equation to predict the in-plane deflection of wood diaphragms. They are presented here in order to exhibit limiting bounds for the actual diaphragm deflection.

The lateral behavior of a wood diaphragm is described in code by the National Design Specification for Wood Construction (NDS). The specification proposes that the lateral deflection of a wood structural panel diaphragm (d in Figure 3-7) under uniform lateral load is:

$$d = \frac{5vL^3}{8EAb} + \frac{vL}{4Gt} + 0.188Le_n + \frac{\sum(\Delta_c X)}{2b} \qquad \text{Eq 3-1}$$

where d is the mid-span deflection, v is the maximum shear, L is the diaphragm length, A is the chord cross-sectional area, b is the diaphragm width, t is the diaphragm thickness, e_n is the nail deformation/slip, and $\Sigma(\Delta_c X)$ is the sum of the individual chord-splice slip values of the diaphragm. The first term in the equation represents the diaphragm deflection due to bending, the second due to shear, the third due to nail deformation or slippage, and the fourth due to chord splice slip. The first two terms evolve from simple bending and shear analysis. The term due to nail deformation is generally far greater than the others and is also the most difficult to accurately determine.

FEMA 356 presents a similar equation for diaphragm deflection. However, it makes a distinction between plywood diaphragms and diagonally sheathed diaphragms. For a single diagonal sheathed diaphragm, the lateral deflection d is:

$$d = {vL}/{2G_d} \qquad \text{Eq 3-2}$$

where G_d is given as 8,000 lb/in. The FEMA 356 equation essentially incorporates all the terms in the NDS equation into one term and defines G_d based on the general characteristics the diaphragm. FEMA defines a typical single diagonal sheathed diaphragm as 1-in. thick sheathing laid at 45 degrees to the framing members and nailed with two or more 8d nails per board at each support.

Finally, Cohen's thesis on Seismic Response of Low-Rise Masonry Buildings includes a stiffness equation for the diaphragm he tested (similar to the one in this study) based on dynamic analysis (Cohen 2001). He determined that the stiffness of the diaphragm is:

$$K = A'G\frac{\pi^2}{2L} \qquad \text{Eq 3-3}$$

where $A'G$ was calculated to be 1,300 kips based on experimental data. Therefore, the deflection can be determined using:

$$d = {V}/{K} \qquad \text{Eq 3-4}$$

where V is the total diaphragm shear. It is important to note that the calculated $A'G$ value is derived for the diaphragm used in the tests (22 ft by 4.67 ft, 4d nailing, and 3/8 in. thick). However, the diaphragm in this study is similar enough to Cohen's that a conversion factor based on the width of the diaphragm can be used. Cohen states that $A'G$ is proportional to diaphragm width; therefore, to convert the $A'G$ value from that for the tested 4.67 ft wide diaphragm to that for

a different width, multiply by the ratio of the new diaphragm width to 4.67 ft. Therefore, for the diaphragm in this study, $A'G$ would equal 3,340 kips.

These equations were then used on Cohen's diaphragm under 2,500 lb of shear to determine their relative accuracy. As seen from Table 3-3, the FEMA equation overpredicts the actual diaphragm deflection, while the NDS equation is much more accurate even though it is supposed to be for a different type of diaphragm. Calculations were also made for the 12 ft by 12 ft diaphragm used in this study under 4,000 lb of shear. Based on the data the deflection of the diaphragm under 4,000 lb of shear should be between 0.035 in. and 0.125 in. For other values of shear, the deflection should be between the Cohen and FEMA calculated values. This approximated stiffness results in a diaphragm frequency between 8.8 and 16.7 Hz.

Table 3-3. Diaphragm deflections

	22'x 4.67'	12'x12'
NDS	0.116"	0.060"
FEMA	0.368"	0.125"
Cohen	0.100"	0.035"
Actual	0.120" *	

*The measured diaphragm deflection includes the deflection of the in-plane shear walls.

Accurate calculation of diaphragm deflection is important because the out-of-plane displacement of the walls is largely controlled by the lateral displacement of the diaphragm. The more the diaphragm deflects, the more the out-of-plane walls will have to deform (Simsir et al. 2001). As mentioned previously, out-of-plane wall failures are common in URM buildings; however, many times failures can be prevented by ensuring that there is a sound connection between the diaphragm and the walls.

Ground Motions

In addition to the characteristics of the building that affect its behavior, the characteristics of the ground motions also play an important role. Three ground motions were considered to cover a range of possible conditions a building might encounter.

Nahanni

The 23 December 1985 Nahanni earthquake occurred in the Northwest Territories of Canada. This ground motion represents an intraplate earthquake that could occur in the Central United States. The response spectrum (Figure 3-8) shows a narrow frequency content at the natural period of the test structure. It also indicates that the earthquake had nearly the same x and y components; therefore, there is little difference in directional behavior. There is also a sharp spike in its time history (Figure 3-9), which may affect the building.

The Nahanni earthquake had a moment magnitude of 6.8. The ground motion chosen was measured at a distance of 6 km from the fault rupture with a site condition of rock (Vs > 600 mps). The earthquake was recorded in two perpendicular horizontal directions, x (NAHANNI/S1280) and y (NAHANNI/S1010), and one vertical direction, up (NAHANNI/S1-UP). The motions were obtained from the Pacific Earthquake Engineering Research (PEER) strong motion database website. They were then modified by multiplying the time scale by $1/\sqrt{2}$ to account for the scale of the test model.

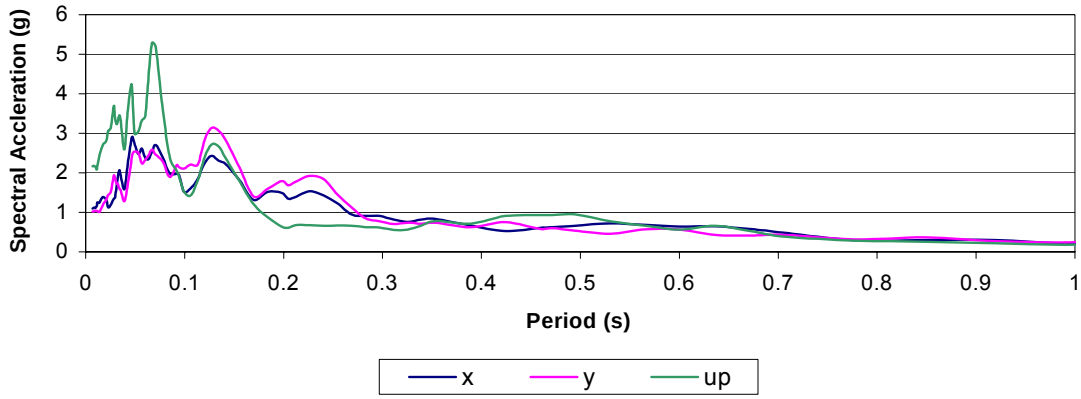

Figure 3-8. Response spectrum for the Nahanni earthquake.

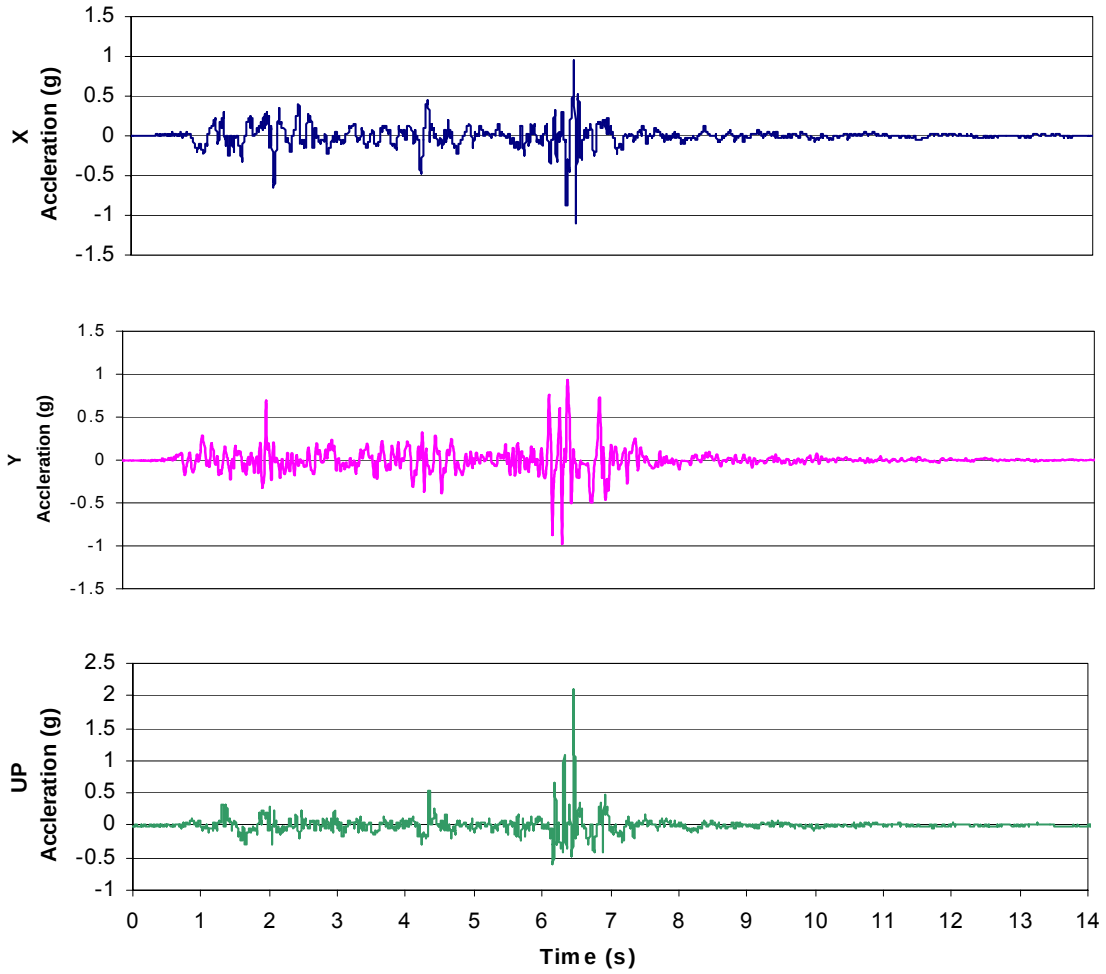

Figure 3-9. Time history for the Nahanni earthquake.

El Centro

The 19 May 1940 Imperial Valley earthquake occurred in Southern California, near the border of Mexico. This ground motion is widely used and well understood. Furthermore, the response spectrum (Figure 3-10) shows a broad frequency content to ensure all modes are excited. It also has different levels of spectral acceleration in the x and y directions that could induce directional responses. The time history of the earthquake is shown in Figure 3-11.

The earthquake had a moment magnitude of 7.0. The ground motion used was measured 8.3 km from the fault rupture with a site condition of deep broad soil (Vs = 180-360 mps). The earthquake was recorded in two perpendicular horizontal directions, x (IMPVALL/I-ELC180) and y (IMPVALL/I-ELC270), and one vertical direction, up (IMPVALL/I-ELC-UP). The motions were obtained from the PEER strong motion database website. These motions were then modified by multiplying the time scale by $1/\sqrt{2}$ to account for the scale of the test model.

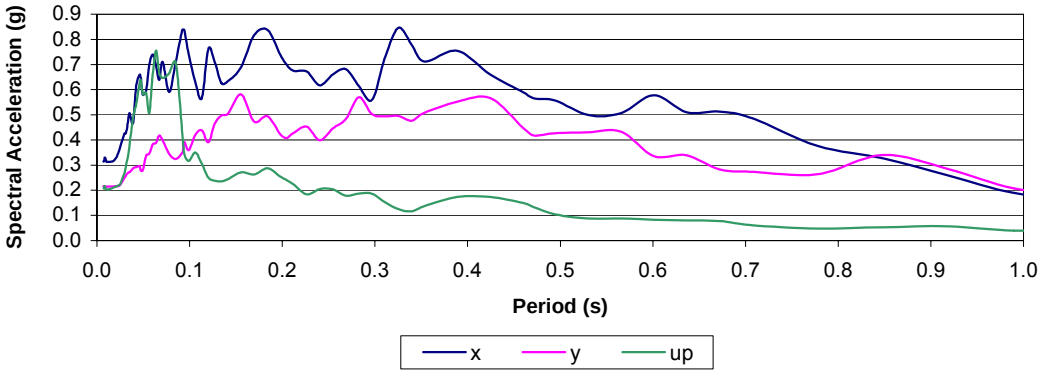

Figure 3-10. Response spectrum for El Centro earthquake.

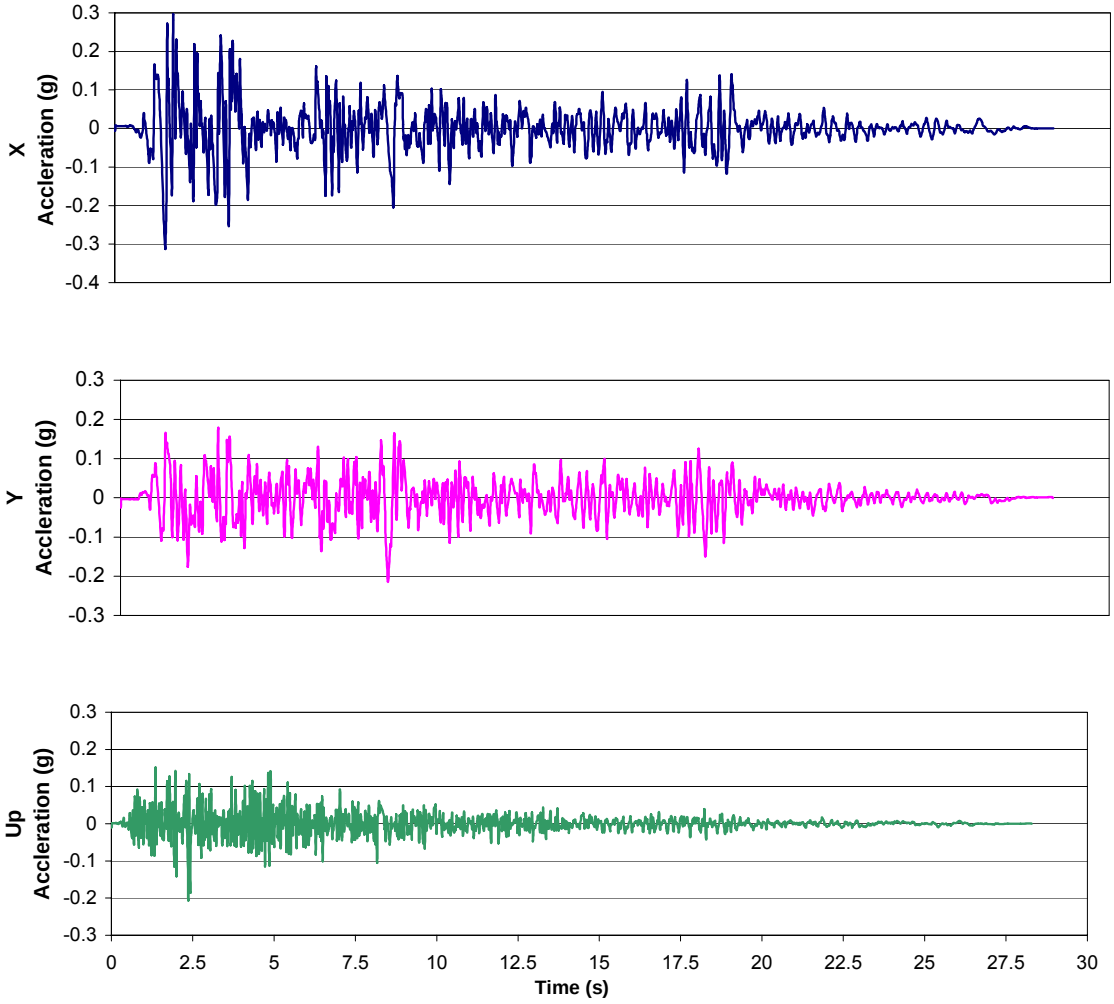

Figure 3-11. Time history for El Centro earthquake.

Loma Prieta

The 18 October 1989 Loma Prieta earthquake occurred near San Francisco, CA. This ground motion was chosen because it shows strong directional behavior. The response spectrum (Figure 3-12) indicates that the peak responses in the x and y directions occur at different periods. Furthermore, it also shows a broad frequency content to ensure all modes are excited. The time history of the earthquake is shown in Figure 3-13.

The earthquake had a moment magnitude of 6.9. The ground motion used is from the Capitola record of the earthquake. It was recorded 14.5 km from the fault rupture with a site condition of deep narrow soil (Vs = 180-360 mps). The earthquake was recorded in two perpendicular horizontal directions, x (LOMAP/CAP000) and y (LOMAP/CAP090), and one vertical direction, up (LOAMP/CAP-UP). The motions were obtained from the PEER strong motion database website. These motions were then modified by multiplying the time scale by $1/\sqrt{2}$ to account for the scale of the test model.

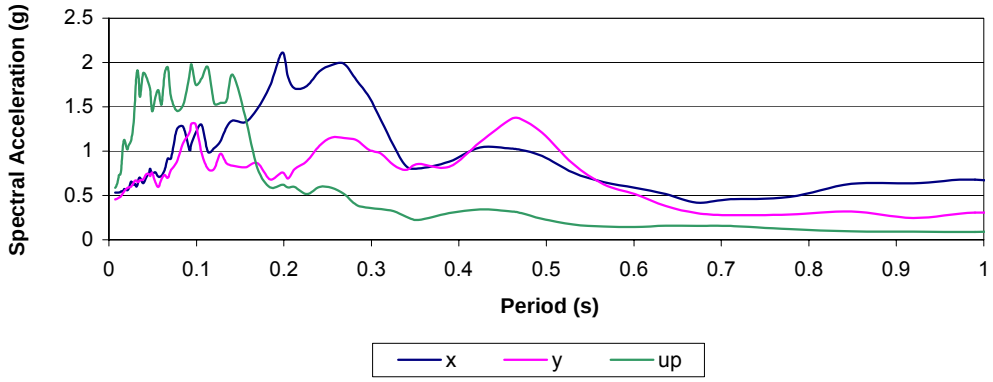

Figure 3-12. Response spectrum for the Loma Prieta earthquake.

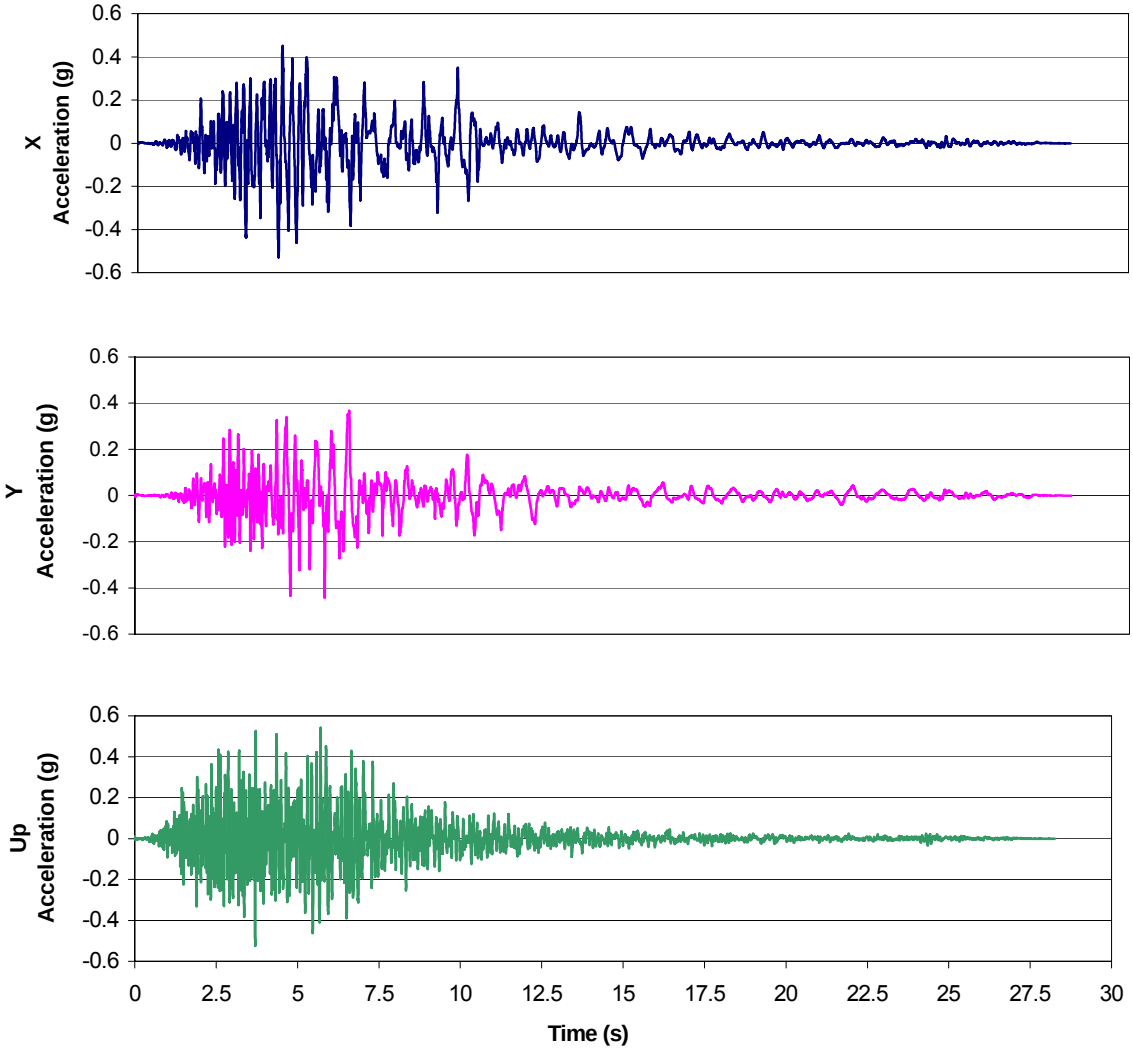

Figure 3-13. Time history for the Loma Prieta earthquake.

4 System Analysis

Several analytical models were developed to predict the dynamic behavior of the test structure. The building system was analyzed using equivalent static, response spectrum, linear time history, and pushover analyses. Each analysis method included careful consideration of the directions of load application. Seismic loads were applied independently along each coordinate axis and simultaneously along all three directions.

Linear-elastic Models

The linear-elastic finite element models of the test structure were created in the Structural Analysis Program 2000 Nonlinear (SAP 2000NL). The models are depicted in Figures 4-1 through 4-4. The walls of the models were constructed of shell elements and were assigned the experimental material properties presented in Chapter 2. The number of shell elements ensures geometric conformity and an accurate description of the response characteristics of the building. The diaphragms of the 3D model were constructed of shell elements representing the diagonal sheathing, while frame elements were used to represent the joists and the stud walls. The diaphragm was calibrated to obtain deflection characteristics in agreement with the results from Chapter 3 by reducing the thickness of the shell element (diaphragm thickness) to 0.0625 in.

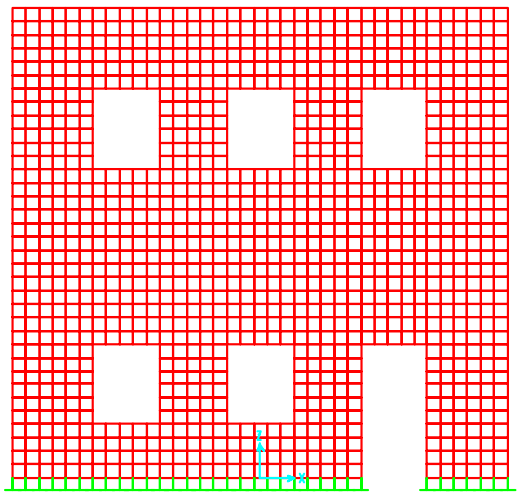

Figure 4-1. 2D SAP model of walls A and B (reverse).

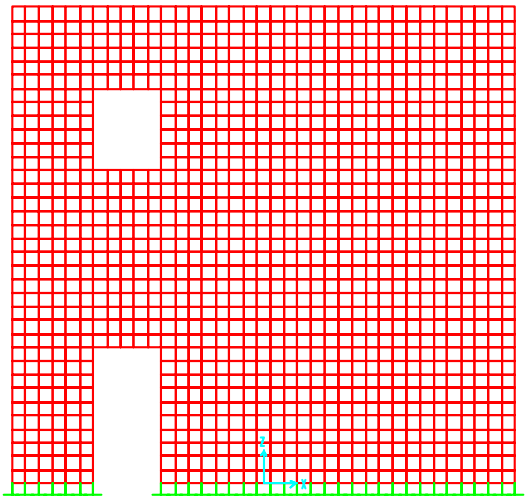

Figure 4-2. 2D SAP model of wall 1.

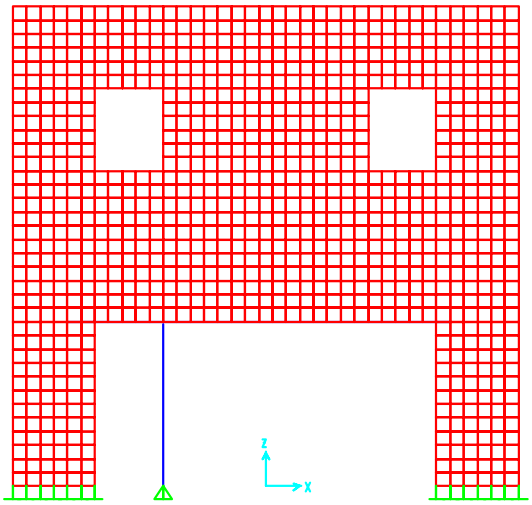

Figure 4-3. 2D SAP model of wall 2.

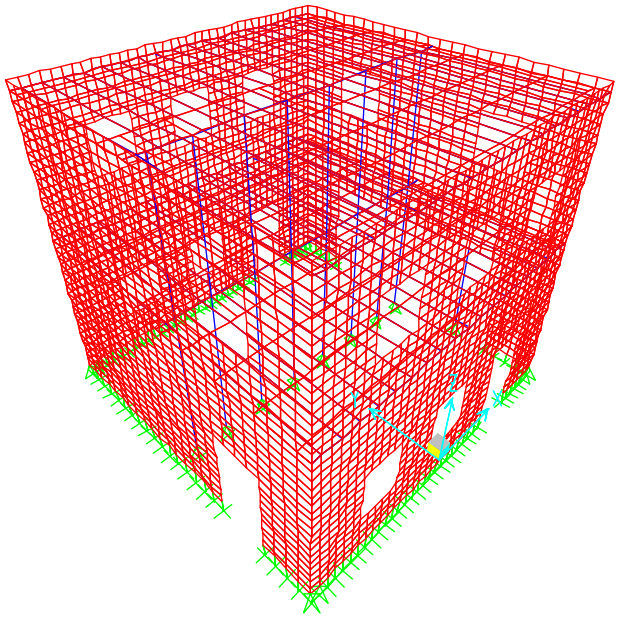

Figure 4-4. 3D SAP model of test structure.*

The 2D models were developed to predict the response of the walls alone (no diaphragm participation) and as a check of the 3D model. The National Earthquake Hazards Reduction Program (NEHRP) "Recommended Provisions for Seismic Regulations for New Buildings and Other Structures," FEMA 368, allows for the use of 2D models provided that there are no torsional irregularities, and that the model accounts for the participation of the diaphragm in the structure's dynamic response. Since these models consider only the added mass of the diaphragm and not its dynamic behavior, they would not be permissible for structural analysis. However, they are presented here in order to examine the inherent behavior of the walls and the effect of vertical motions on that behavior. The 3D model does meet the requirements of FEMA 368, and can be used to predict the behavior of the building system.

Finite element linear-elastic analysis allows for an accurate determination of structural response only until first cracking. Regardless of this limitation, it determines the stress distribution throughout the model, facilitating the identification of stress concentrations where the first cracks would develop. Therefore, by examining the stress state of the structure under various combinations of vertical and lateral loading, the 3D behavior of the building can be understood. Post-cracking behavior is examined by pushover analysis.

Linear Static Analysis

Static analysis is one of the simplest methods used to analyze a structure. Although it cannot determine the dynamic characteristics of a building, it can be used to estimate the response of the structure to an equivalent lateral load.

The equivalent lateral force procedure, presented in Section 5.4 of FEMA 368, consists of the application of equivalent lateral static forces acting on a linear model of the structure. The equivalent forces are calculated based on the assumption that all of the structure's mass is active in the first mode. In this procedure, the total base shear can be computed from Equations 4-1 and 4-2:

$$V = C_s W \quad \text{Eq 4-1}$$

$$C_s = \frac{S_{DS}}{R/I} \quad \text{Eq 4-2}$$

where V is the total base shear, C_s is the seismic response coefficient, W is the weight of the building, S_{DS} is the design spectral response acceleration, R is the response modification factor, and I is the occupancy importance factor (1.0). The response modification factor given in FEMA 368 for ordinary plain masonry shear walls is 1.5. Once the base shear has been determined, it is distributed over the height of the structure in accordance with Equations 4-3 and 4-4:

$$F_x = C_{vx} V \quad \text{Eq 4-3}$$

$$C_{vx} = \frac{w_x h_x^{\,k}}{\sum_{i=1}^{n} w_i h_i^{\,k}} \quad \text{Eq 4-4}$$

where F_x is the lateral force applied at level x, C_{vx} is the vertical distribution factor at level x, w_i and w_x are the portions of gravity load assigned to levels i and x, h_i and h_x are the heights from the base to levels i and x, and k is equal to 1.0 for the test model. S_{DS} values determined from the time histories used in this study are shown in Table 4-1. The distribution of static load on the structure based on a unit S_{DS} value is shown in Table 4-2.

Table 4-1. S_{DS} values for ground motions

	x	y	Vertical
Nahanni	2.2 g	2.20 g	3.60 g
El Centro	0.7 g	0.45 g	0.63 g
Loma Prieta	1.4 g	0.97 g	1.70 g

Table 4-2. Vertical distribution of equivalent seismic force (based on S_{DS} = 1g)

	Fx (kip)		
Height (in.)	**Wall AB**	**Wall 1**	**Wall 2**
132.6	7.45	2.98	2.98
108.6	2.66	2.49	2.16
84.6	3.17	2.16	2.12
72.6	1.65	0.00	0.00
60.0	2.31	1.56	1.50
36.0	0.95	0.84	0.30
12.0	0.37	0.27	0.10

With the static force distribution calculated from the FEMA 368 procedure, the linear-elastic finite element models were used to determine the structural response. SAP 2000NL was used to perform the analysis. See the results section of this chapter for details.

Linear Dynamic Analysis

Linear dynamic analysis considers the dynamic characteristics of the structure to determine the overall behavior of the building. Modal analysis calculates and superposes the response for each mode, while time-history analysis calculates the response for discrete time steps based on the equation of motion.

Modal Response Spectrum Analysis

The modal response spectrum analysis procedure, presented in Section 5.5 of FEMA 368, is based upon the superposition of the responses from individual modes. Each mode can be represented by a single degree of freedom oscillator with its own mass, stiffness, and damping. The equivalent lateral force procedure is similar to modal analysis, except that the latter considers higher mode responses. As a result, the analysis equations are analogous to those presented in the previous section, but are generalized for any mode. The total base shear can be calculated for a given mode, *m*, using Equation 4-5:

$$V_m = C_{sm}\overline{W}_m \qquad \text{Eq 4-5}$$

where C_{sm} is the modal seismic response coefficient and $\overline{W}_m$ is the modal weight of the building. These two terms can be determined from Equations 4-6 and 4-7:

$$C_{sm} = \frac{S_{am}}{R/I} \qquad \text{Eq 4-6}$$

$$\overline{W}_m = \frac{\left(\sum_{i=1}^{n} w_i \phi_{im}\right)^2}{\sum_{i=1}^{n} w_i \phi_{im}{}^2} \qquad \text{Eq 4-7}$$

where S_{am} is the design spectral response acceleration at the modal period T_m determined from the response spectrum, R is the response modification factor (1.5), I is the occupancy importance factor (1.0), w_i is the portion of gravity load assigned to level i, and ϕ_{im} is the modal displacement.

The response spectrums used in this analysis came from the time histories of the recorded ground motions presented in Chapter 3. SAP 2000NL automatically calculates the modal periods, weights, and spectral accelerations. The modal results are then combined using the CQC (complete quadratic combination) rule, which accounts for statistical coupling between closely spaced modes. See the results section of this chapter for details.

Linear Response History Analysis

Another type of linear dynamic analysis is the linear response history analysis procedure, which is commonly referred to as time-history analysis. The method, presented in Section 5.6 of FEMA 368, predicts structural response at discrete time steps by satisfying the equation of motion. As a result, response quantities can be calculated at any time location throughout the duration of an earthquake. This facilitates the comparison of structural behavior for different ground motions, in addition to examining the effects of various directional and combinational load cases.

This analysis used the models presented at the beginning of this chapter and the time histories of the ground motions presented in Chapter 3. The analysis was performed using SAP 2000NL. See the results section of this chapter for details.

Results of Linear Analysis

The results for the 2D linear-elastic models are presented in Tables 4-3 through 4-5. The seismic loads were applied independently in the x (in-plane) and z (vertical) directions, and also simultaneously (xz). The models were analyzed by the three types of linear analysis presented earlier: equivalent static, response spectrum, and time history. For each type of analysis, the maximum displacement at any point in time for the top right corner of the wall is given in inches. Displacements are given in both the vertical and horizontal directions. Also for each type of analysis, the maximum total force at the base of the wall is given in the horizontal (shear) and vertical directions. The vertical forces include the dead weight of the wall and are presented as the maximum force / the minimum force. A negative number for the minimum force indicates that the wall is in tension. The static analysis procedure did not consider vertical forces; therefore, the vertical forces indicate the dead weight of the walls.

The linear time history and response spectrum methods produced similar results in almost every case. In contrast, the static method predicted displacements and base forces that were up to three times larger than those determined by the dynamic methods. This discrepancy seems to indicate that the assumption that the walls are responding only in the first mode is not always reasonable. Since experimental data are not yet available, it is impossible to say how accurate the dynamic methods are or if the static method is too conservative. However, the equivalent lateral force procedure is overly conservative at worst and a good predictor of structural response at best, which seems acceptable for a simple design method. In addition, the agreement in results between the time history and response spectrum analyses indicates that they are comparable approaches.

For all analysis types, the responses for the independent x motion were nearly the same as the responses for the combined xz motion, except for the vertical base force. In this case, the structural behavior was almost identical to the independent z response. This indicates that, for bi-directional loading, the response of the walls can be determined from the maximum response from the independently applied uni-directional loads.

Examination of the forces and displacements resulting from the different ground motions (Tables 4-3 through 4-5) shows clearly that the Nahanni earthquake would have the most damaging effects. It produced the largest responses for each wall for the horizontal, vertical, and bi-directional loading cases. In addition, the static analysis results were most comparable to the dynamic analyses for the Nahanni motion, perhaps indicating the presence of a strong first mode response, as predicted in Chapter 3.

Table 4-3. Displacements and base forces from 2D linear-elastic models under Nahanni ground motion

Nahanni

Wall AB

	Displacement (in)						Base Force (kip)					
	Static		Response Spectrum		Linear Time History		Static		Response Spectrum		Linear Time History	
Motion	horizontal	vertical	horizontal	vertical	horizontal	vertical	horizontal	vertical	horizontal	vertical	horizontal	vertical
xz	0.1074	-0.0345	0.0761	-0.027	0.0762	-0.0254	44.2	18.38	31	41.2/-4.4	32.17	40.7/11.2
x	0.1074	-0.0345	0.0762	-0.02618	0.07625	-0.0255	44.17	18.38	31	18.65	32.2	18.65
z	0	-0.0044	0.0007	-0.01062	0.00063	-0.01065	0	18.38	0.392	41.2/-4.4	0.211	40.8/-11.0

Wall 1

	Displacement (in)						Base Force (kip)					
	Static		Response Spectrum		Linear Time History		Static		Response Spectrum		Linear Time History	
Motion	horizontal	vertical	horizontal	vertical	horizontal	vertical	horizontal	vertical	horizontal	vertical	horizontal	vertical
xz	0.0478	-0.0206	0.0268	-0.0153	0.0231	-0.0158	22.63	11.08	10.83	34.6/-12.4	11.48	36.9/4.2
x	0.0478	-0.0206	0.0267	-0.0132	0.0234	-0.0114	22.63	11.08	10.54	12.61	11.08	11.11
z	0.000051	-0.00266	0.00211	-0.00975	0.00211	-0.00949	0	11.08	2.508	34.6/16.6	0.689	36.5/4.13

Wall 2

	Displacement (in)						Base Force (kip)					
	Static		Response Spectrum		Linear Time History		Static		Response Spectrum		Linear Time History	
Motion	horizontal	vertical	horizontal	vertical	horizontal	vertical	horizontal	vertical	horizontal	vertical	horizontal	vertical
xz	0.1432	-0.0222	0.1373	-0.0315	0.1372	-0.0265	20.1	6.98	19.44	25.0/-10.6	17.21	27.1/1.3
x	0.1432	-0.0222	0.137	-0.0201	0.1368	-0.0205	20.1	6.98	19.41	7.08	17.41	7.04
z	0	-0.00587	0.00505	-0.0272	0.0022	-0.0246	0	6.98	1.03	24.3/-10.3	0.438	27.2/1.34

Table 4-4. Displacements and base forces from 2D linear-elastic models under El Centro ground motion

El Centro

Wall AB

	Displacement (in)						Base Force (kip)					
	Static		Response Spectrum		Linear Time History		Static		Response Spectrum		Linear Time History	
Motion	horizontal	vertical	horizontal	vertical	horizontal	vertical	horizontal	vertical	horizontal	vertical	horizontal	vertical
xz	0.0342	-0.014	0.0181	-0.00963	0.0181	-0.00743	14.06	18.38	7.32	20.17/16.6	7.88	19.9/16.4
x	0.0342	-0.014	0.0181	-0.00961	0.0179	-0.00739	14.06	18.38	7.32	18.44	7.87	18.56
z	0	-0.0044	0.0009	-0.00493	0.0008	-0.0048	0	18.38	0	20.2/16.6	0.018	19.8/11.0

Wall 1

	Displacement (in)						Base Force (kip)					
	Static		Response Spectrum		Linear Time History		Static		Response Spectrum		Linear Time History	
Motion	horizontal	vertical	horizontal	vertical	horizontal	vertical	horizontal	vertical	horizontal	vertical	horizontal	vertical
xz	0.00938	-0.00633	0.00593	-0.0049	0.00558	-0.00403	4.63	11.08	2.18	12.9/9.2	2.55	12.6/8.9
x	0.00938	-0.00633	0.00592	-0.00488	0.00554	-0.00405	4.63	11.08	2.17	11.29	2.54	11.11
z	0.00051	-0.00266	0.00083	-0.00323	0.00073	-0.00306	0	11.08	0.225	12.9/9.2	0.061	12.6/8.9

Wall 2

	Displacement (in)						Base Force (kip)					
	Static		Response Spectrum		Linear Time History		Static		Response Spectrum		Linear Time History	
Motion	horizontal	vertical	horizontal	vertical	horizontal	vertical	horizontal	vertical	horizontal	vertical	horizontal	vertical
xz	0.0293	-0.00923	0.0221	-0.00863	0.0222	-0.00784	4.11	6.98	3.13	8.3/5.7	3.18	8.2/5.6
x	0.0293	-0.00923	0.0222	-0.00817	0.0222	-0.00748	4.11	6.98	3.13	7.08	3.18	7.04
z	0	-0.00587	0.0041	-0.0074	0.00073	-0.007	0	6.98	0.007	8.25/5.8	0.009	8.2/5.6

Table 4-5. Displacements and base forces from 2D linear-elastic models under Loma Prieta ground motion

Loma Prieta

Wall AB

	Displacement (in)						Base Force (kip)					
	Static		Response Spectrum		Linear Time History		Static		Response Spectrum		Linear Time History	
Motion	horizontal	vertical	horizontal	vertical	horizontal	vertical	horizontal	vertical	horizontal	vertical	horizontal	vertical
xz	0.0683	-0.0235	0.0208	-0.0109	0.02	-0.00941	28.12	18.38	8.48	27.6/9.2	8.32	41.3/-6.8
x	0.0683	-0.0235	0.0207	-0.01041	0.0199	-0.0096	28.12	18.38	8.48	18.47	8.29	18.43
z	0	-0.0044	0.000288	-0.0062	0.00095	-0.00704	0	18.38	0.151	27.6/9.2	0.581	41.3/-6.28

Wall 1

	Displacement (in)						Base Force (kip)					
	Static		Response Spectrum		Linear Time History		Static		Response Spectrum		Linear Time History	
Motion	horizontal	vertical	horizontal	vertical	horizontal	vertical	horizontal	vertical	horizontal	vertical	horizontal	vertical
xz	0.0208	-0.0106	0.0135	-0.00854	0.0131	-0.00684	9.98	11.08	4.87	20.36/1.8	5.31	21.04/4.5
x	0.0208	-0.0106	0.0135	-0.00785	0.0126	-0.00745	9.998	11.08	5.2	11.59	4.68	11.21
z	0.00051	-0.00266	0.00174	-0.00323	0.00177	-0.00306	0	11.08	1.045	20.3/1.81	0.775	21.0/4.4

Wall 2

	Displacement (in)						Base Force (kip)					
	Static		Response Spectrum		Linear Time History		Static		Response Spectrum		Linear Time History	
Motion	horizontal	vertical	horizontal	vertical	horizontal	vertical	horizontal	vertical	horizontal	vertical	horizontal	vertical
xz	0.0631	-0.0131	0.0444	-0.0147	0.0444	-0.0133	8.26	6.98	6.29	13.4/0.8	5.99	13.5/1.5
x	0.0631	-0.0131	0.0444	-0.0105	0.0443	-0.0103	8.86	6.998	6.27	7.08	5.95	7.04
z	0	-0.00587	0.00185	-0.0134	0.0011	-0.0124	0	6.98	0.373	13.1/0.8	0.22	13.5/1.5

An important feature of URM behavior not present in the analysis results is the variation in behavior of the wall due to a change in vertical stress. As described in Chapter 3, a significant decrease in vertical stress will decrease the strength of the wall, and the horizontal displacements would increase when both directions of motion are considered. This dependency could not be included in the linear-elastic SAP 2000 models.

Since the results for the response spectrum and time-history analyses were very similar for the 2D models, only a time-history analysis was conducted for the 3D model. It was chosen because it determines the response of the structure throughout the duration of the earthquake, which allows for an in-depth investigation of the effects of directional loading. Results from the 3D model analysis are shown in Table 4-6, and Figures 4-5 through 4-8. Table 4-6 presents the x, y, and z displacements at roof level for the four corners of the building. A diagram of the corner locations is shown in Figure 4-5. In addition, the diagram shows the orientation of the coordinate system used. The displacements were determined for ground motions applied independently in the x, y, and z directions, as well as applied simultaneously in all three directions (xyz). They are the maximum displacements calculated for each specified time history.

Figures 4-6 through 4-8 give the total force at the base of each wall for the following cases: maximum shear force, maximum compressive force, and maximum tensile force. The figures represent a plan view of the building, with walls A and B on the bottom and top, and walls 1 and 2 on the left and right, respectively. Each force is the maximum force at any moment in time and does not occur concurrently with the other forces around the same box. The vertical forces shown include the dead load in the walls, which, for comparison purposes, are given at the bottom of the figures. Results are presented for x, y, and xyz ground motions for the maximum shear case and x, y, z, and xyz for maximum compressive and tensile cases. The notation for vertical forces is positive for compressive and negative for tensile.

The results for the 3D analysis indicate that the majority of the combined xyz responses can be attributed to the response from one direction of motion. There are instances, however, where this attribution is not possible due to the 3D response of the structure. These instances will be discussed in Chapter 5.

Table 4-6. Displacements at building corners from 3D linear-elastic model under time history analysis

Nahanni

	Displacement (in)											
	1			2			3			4		
Motion	x	y	z	x	y	z	x	y	z	x	y	z
x	-0.069	0.00585	-0.0158	-0.0693	0.00723	-0.0166	-0.0702	-0.00797	-0.01681	-0.06981	-0.0089	-0.01482
y	0.01814	0.06766	-0.0153	0.00681	0.1892	-0.00999	0.00857	0.1857	-0.01081	-0.01928	0.06767	-0.02006
z	0.00447	0.0008	-0.00547	0.00343	0.00696	-0.01462	0.00542	-0.00639	-0.01612	0.00621	-0.00166	-0.00399
xyz	0.0771	0.0697	-0.0249	0.0704	0.1846	-0.0157	0.0651	0.1901	-0.0214	0.0581	0.064	-0.0176

El Centro

	Displacement (in)											
	1			2			3			4		
Motion	x	y	z	x	y	z	x	y	z	x	y	z
x	0.02563	0.00237	-0.0083	0.02588	0.00361	-0.00851	0.0254	0.00361	-0.0088	0.02507	0.00317	-0.00757
y	0.0424	0.0137	-0.00611	0.00178	0.03682	-0.00576	0.00273	0.0349	-0.00596	0.00493	0.01363	-0.00663
z	0.00147	0.00017	-0.00371	0.00115	0.0013	-0.00526	0.00158	-0.00133	-0.00564	0.00193	0.000418	-0.00331
xyz	0.0262	0.0139	-0.00874	0.02601	0.0365	-0.00846	0.02561	0.0349	-0.00876	0.02551	0.01321	-0.00801

Loma Prieta

	Displacement (in)											
	1			2			3			4		
Motion	x	y	z	x	y	z	x	y	z	x	y	z
x	0.04911	0.00365	-0.00112	0.04864	0.0044	-0.01353	0.04905	0.0051	-0.01376	0.04935	0.00564	-0.01016
y	0.001174	0.0462	-0.01279	0.0042	0.1237	-0.00878	0.00724	0.1276	-0.00844	0.01478	0.04625	-0.0147
z	0.0028	0.00038	-0.00455	0.00257	0.00296	-0.00797	0.00325	0.00291	-0.00866	0.00355	0.000777	-0.0038
xyz	0.0512	0.0471	-0.0163	0.0493	0.1231	-0.0135	0.048	0.124	-0.01603	0.04656	0.0462	-0.0153

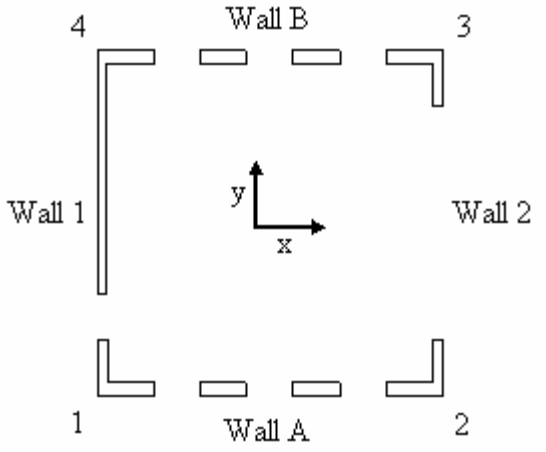

Figure 4-5. Locations of corners.

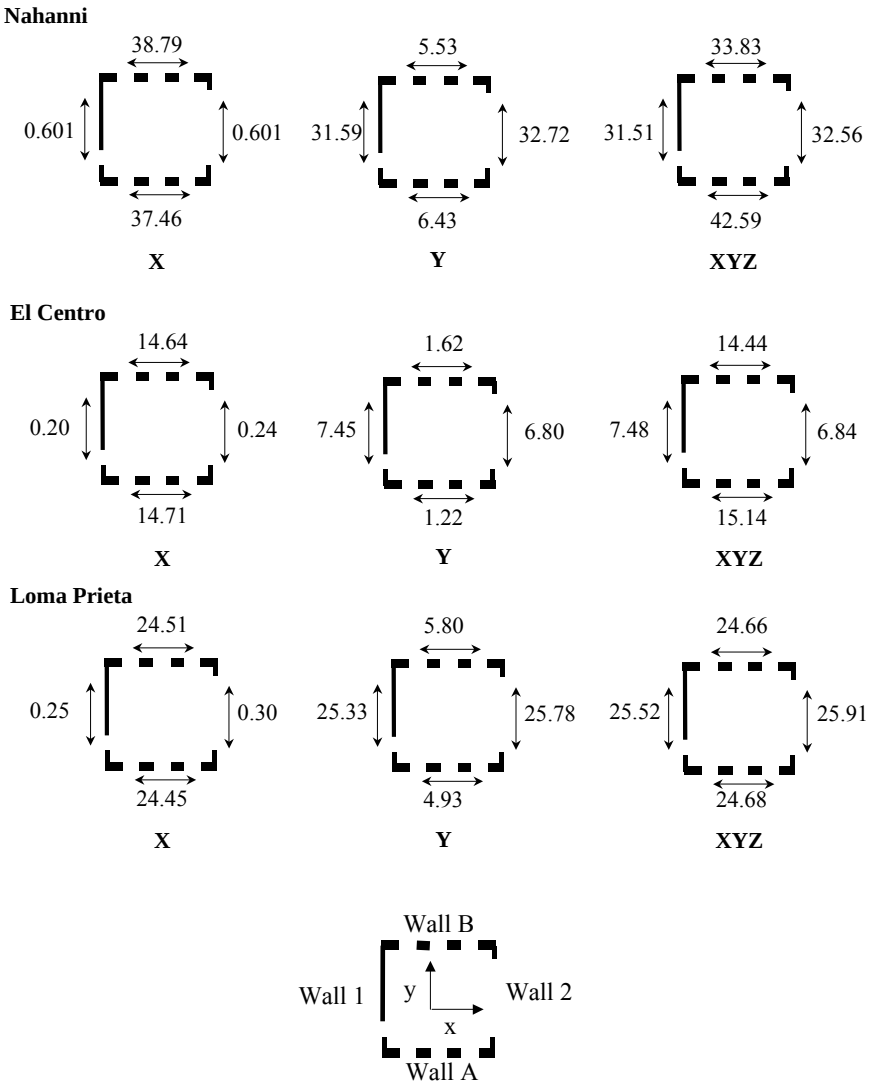

Figure 4-6. Base shears from 3D linear-elastic time history (kip).

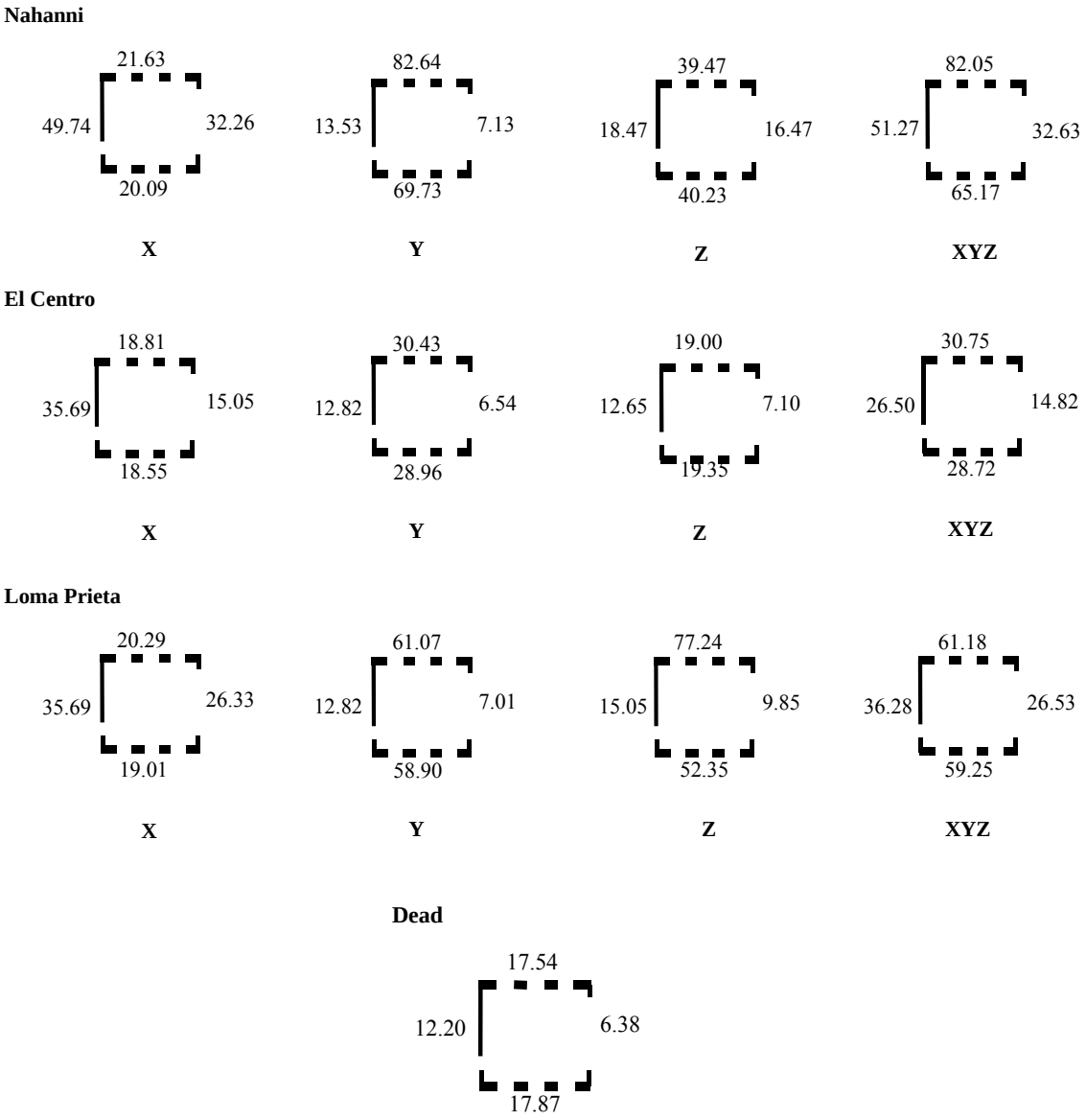

Figure 4-7. Vertical compressive forces from 3D linear-elastic time history (kip).

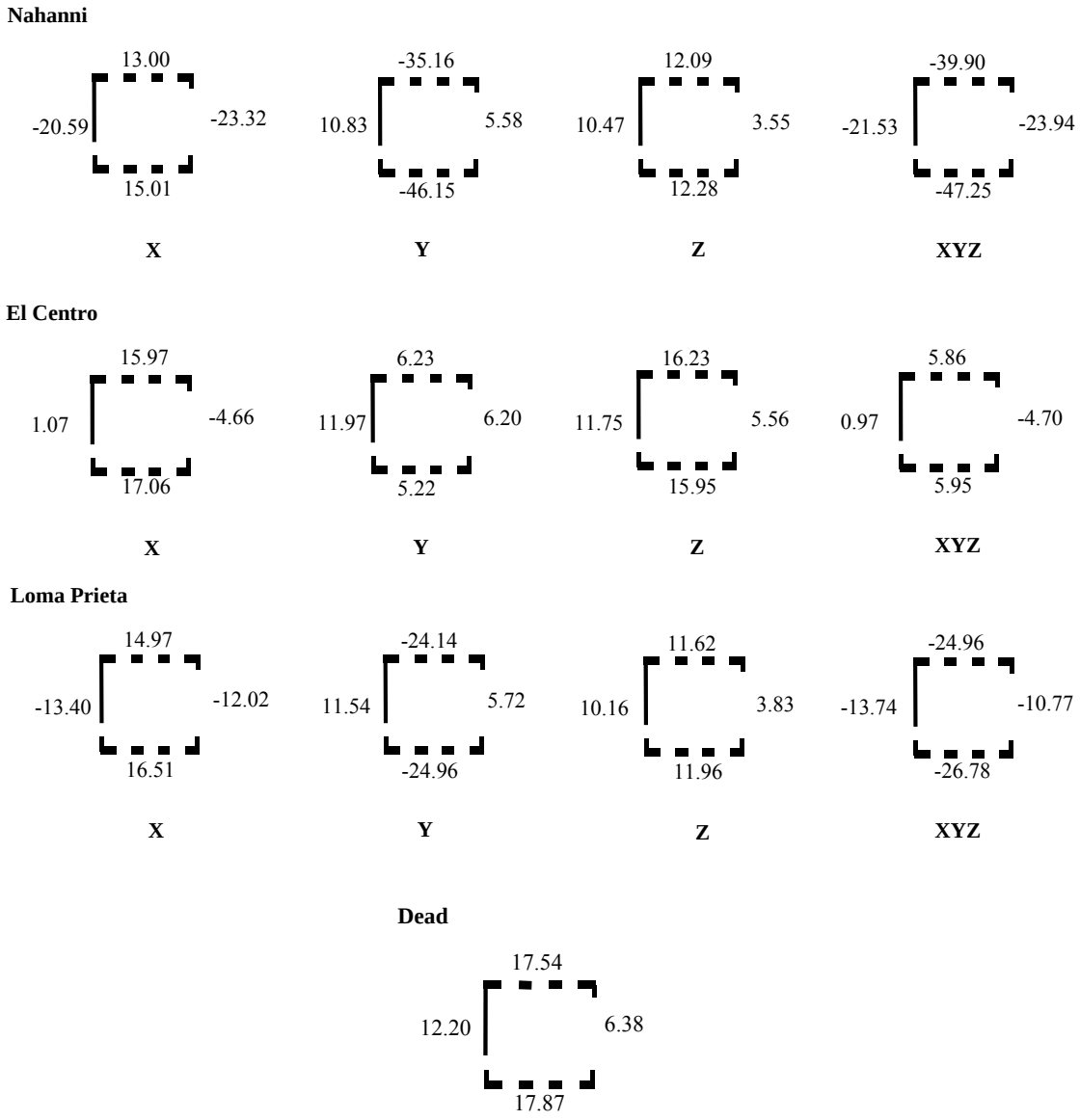

Figure 4-8. Vertical tensile forces from 3D linear-elastic time history (kip).

Pushover Analysis

A pushover analysis consists of a nonlinear model of a structure that is subjected to increasing levels of lateral load. A nonlinear model is unique from a linear model because it can account for the redistribution of forces due to yielding. The result of the analysis is a pushover curve, in which the total base shear applied to the structure is plotted versus a chosen "control displacement" at each load increment. The selected control point is usually located at the top of the structure. This analysis allows for the determination of the force-deformation characteristics of the structure as well as the damage states for various levels of base shear. The method is presented in FEMA 368 as an appendix to Chapter 5.

To perform a pushover analysis, the nonlinear load-deformation response must be specified for each structural element that could potentially yield. In Chapter 3, the nonlinear behavior of individual piers was found based on FEMA 356, and this information was used to assign hinge properties for models created in SAP 2000NL. The lateral pushover loads applied were proportional to the first mode of each wall for the 2D cases and to the fundamental mode of the structure in each horizontal direction for the 3D cases, per FEMA 368 specifications. In addition, the SAP pushovers include the dead load of the test model and P-delta effects.

The results from the SAP 2D analyses are shown in Figures 4-9 through 4-11. Also shown on the figures is the combined pier response (designated as FEMA), calculated by adding the load-deformation relationships for each of the first story piers for a given wall (the second story piers are assumed to not yield). Note that the displacement plotted from SAP is generated at the joint located at the top of the first story piers at the edge of the wall under consideration (for wall 1, this is the height of the building since pier 9 is considered to be a cantilevered pier). If the SAP pushovers for walls A, B, and 2 were plotted based on the displacement of a point at the top of the building, the deformation would be somewhat larger due to global overturning moment. As can be seen from the figures, the combined pier response closely matches the results from the pushover analysis.

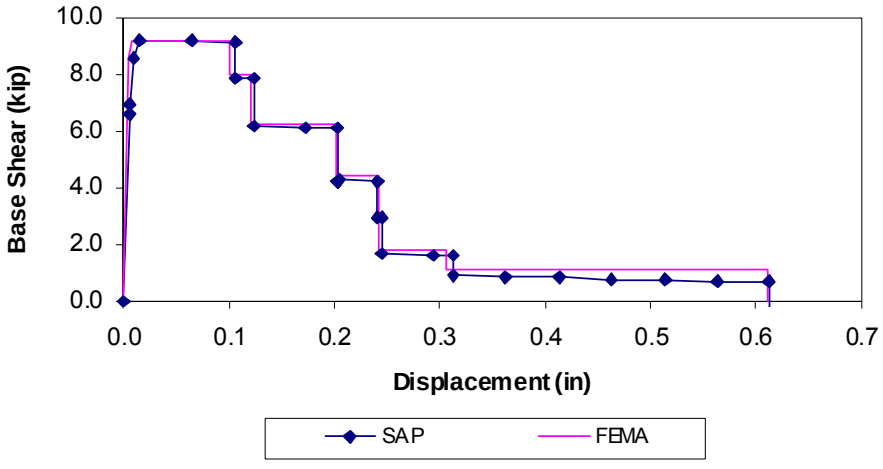

Figure 4-9. Force-deformation relationships for walls A and B.

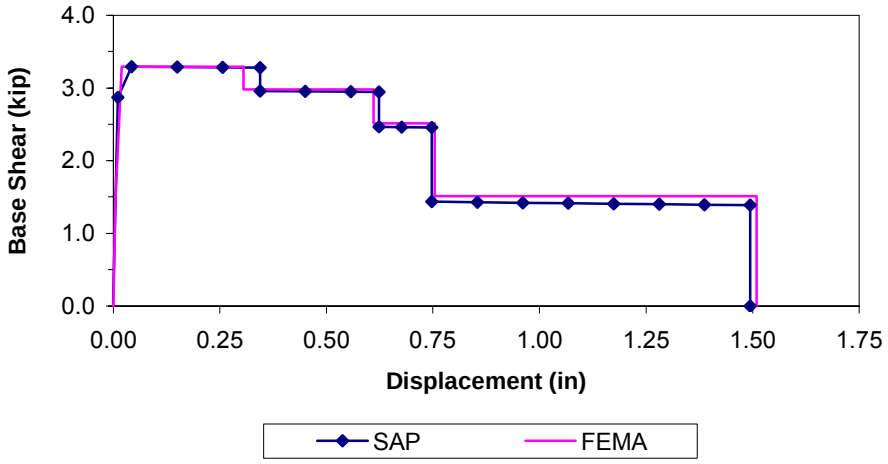

Figure 4-10. Force-deformation relationship for wall 1.

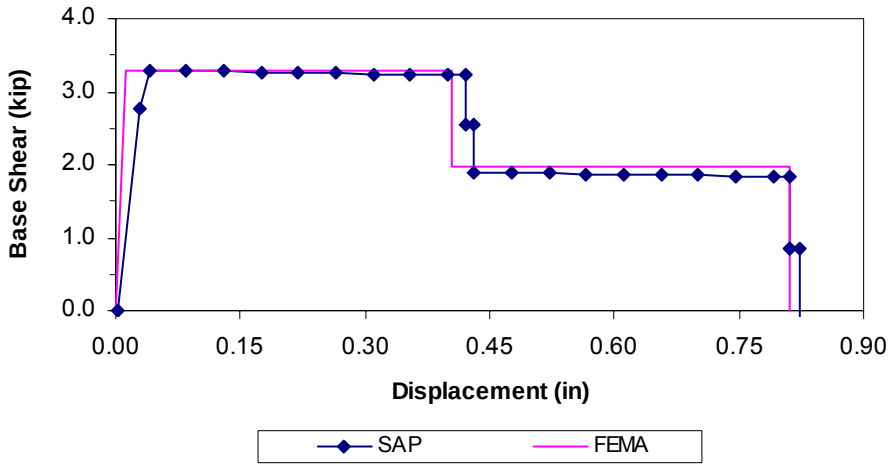

Figure 4-11. Force-deformation relationship for wall 2.

Section 5A.1.1 of FEMA 368 states that "for structures having plan irregularities…or structures without independent orthogonal systems, a three-dimensional model incorporating a minimum of three degrees of freedom, consisting of translation in two orthogonal plan directions and torsional rotation…shall be used." Adhering to FEMA 368, the test model would require analysis using a 3D model. A 3D model of the test structure was created and, in accordance with Section 5A.1.2, pushovers were performed in both horizontal directions. The results of the 3D pushovers are plotted in Figures 4-12 and 4-13 with the combined SAP 2D wall pushovers. The pushover curves for the 3D cases were determined by averaging the response at the tops of the two in-plane walls for the direction under consideration.

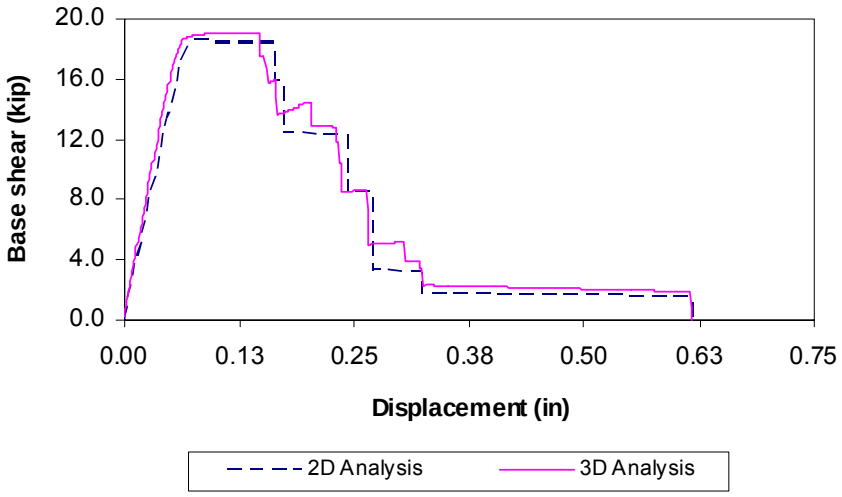

Figure 4-12. Comparison of 2D and 3D pushover curves for walls A and B.

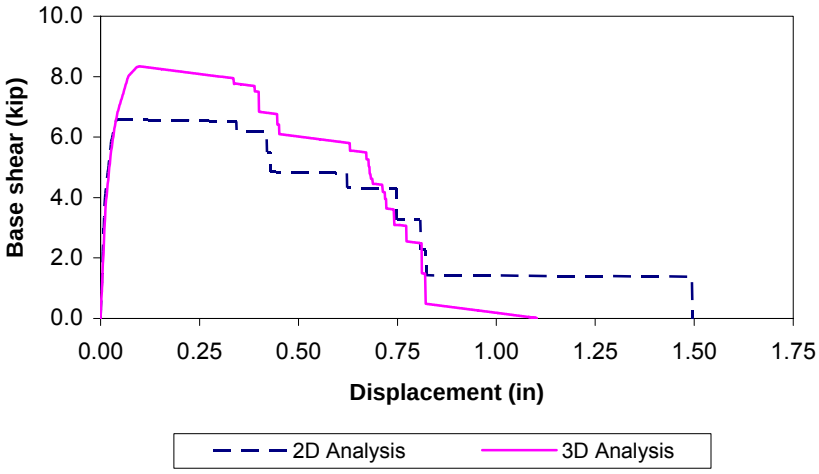

Figure 4-13. Comparison of 2D and 3D pushover curves for walls 1 and 2.

As would be expected, the 3D pushovers exhibit increased strength. This effect is due to the behavior of the out-of-plane walls, which is usually neglected for masonry design. For the pushovers shown above, the out-of-plane strength of the masonry piers was specified in SAP to be one-tenth the in-plane strength. Since the combined in-plane strength of walls A and B are about three times larger than that of walls 1 and 2, the effect of the out-of-plane walls is considerably more pronounced for loading in the 1-2 plane direction.

A predominant feature of the 3D pushover curve for walls 1 and 2 is a reduced deformation capacity compared to that of the 2D response. This behavior is a result of the P-delta effect, or a magnification of the overturning moment caused by lateral deflection of the structure. As the building translates, the downward force due to its own mass becomes eccentric to its base, producing a moment that

combines with that caused by the lateral force. While both the 3D and 2D analyses include P-delta effects, the additional mass from the diaphragm and out-of-plane walls in the 3D model results in a much greater amplification. The weight of the building is just one of two contributing factors in evaluating the severity of P-delta effects, however. If the displacement of the structure is small enough, the effect will be minimal regardless of the vertical compressive force; such is the case for walls A and B. Figures 4-14 and 4-15 show the 3D pushover curves for both horizontal directions, including P-delta effects and neglecting P-delta effects.

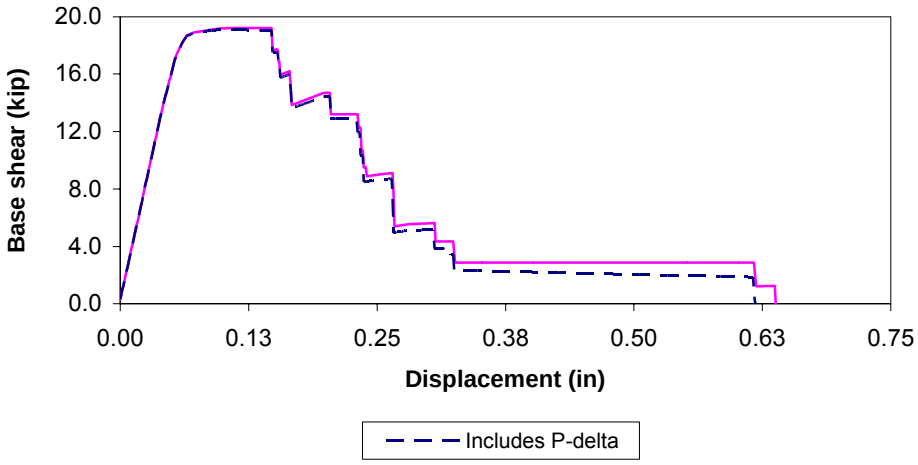

Figure 4-14. P-delta effects for A-B plane direction.

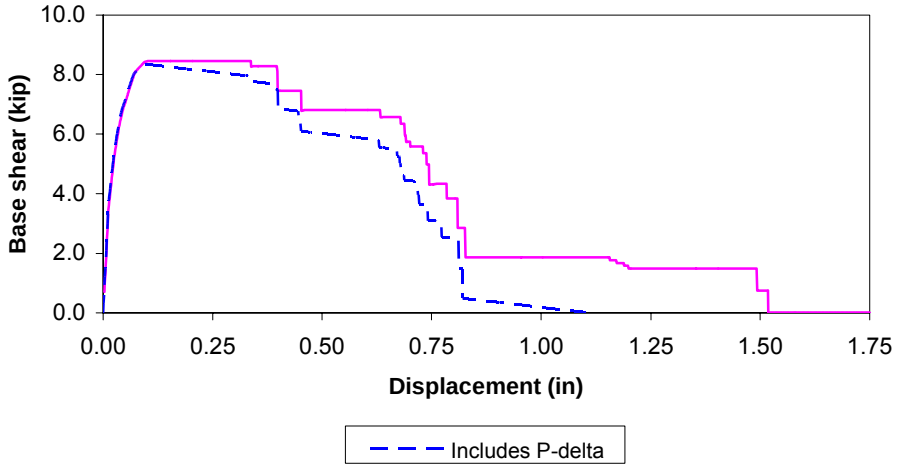

Figure 4-15. P-delta effects for 1-2 plane direction.

5 Evaluation of Response

The responses of the components and building system are evaluated based on the objectives of this study:

- Investigate the effect of tri-directional base motions on the test model.
- Examine dynamic amplification in systems with flexible diaphragms.
- Verify the extrapolation of individual component behavior to the overall response of the building system.
- Provide fundamental knowledge needed to develop seismic protection design.

Tri-directional Responses

This section presents an evaluation of the effects of tri-directional seismic motions on the behavior of a URM building system. In particular, the evaluation considers base shears, vertical forces, and their combined effects.

Base Shears

Determining the load path for a given structure is crucial in understanding its behavior. For the test model, the lateral inertial loads resulting from earthquake excitation are transferred from the diaphragms to the in-plane walls, and finally to the ground. As stated in Chapter 3, the diaphragm in the test model is flexible. Therefore, it distributes load to an in-plane wall according to the tributary mass of the diaphragm and out-of-plane walls. At the diaphragm levels, the distribution of mass is fairly symmetric about the centerlines of the horizontal plan directions. Consequently, it would be expected that, for uni-directional loading in either horizontal direction, the base shears in the in-plane walls are approximately equal.

As an example, see Figures 5-1 and 5-2, which use the Loma Prieta earthquake to compare the base shear for the in-plane walls for the A-B plane direction and 1-2 plane direction, respectively. The figures clearly indicate that the in-plane wall base shears are equal for both cases, confirming the diaphragm's flexibility. In contrast, Figure 5-3 presents the base shear in walls 1 and 2 for the Loma Prieta earthquake when the diaphragm is modeled as rigid. The plot shows that,

due to the rigidity of the diaphragm, the applied base shear is distributed in proportion to the stiffness of the walls.

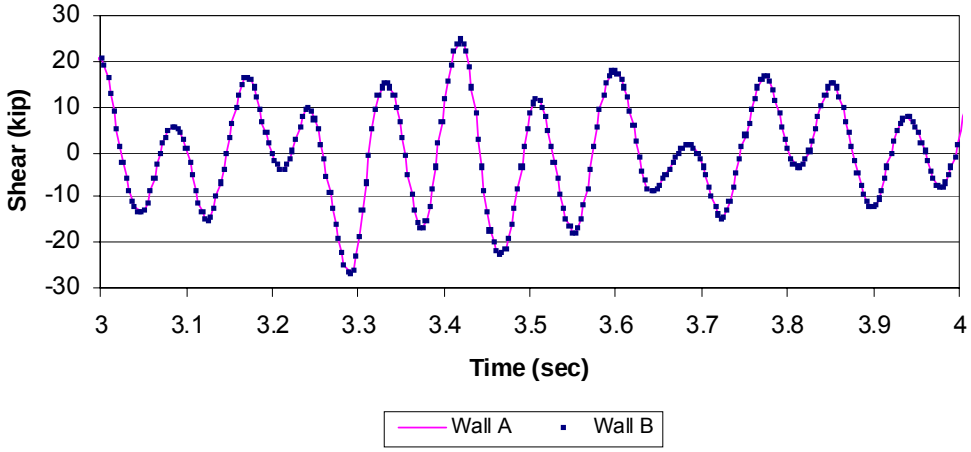

Figure 5-1. Base shears on walls A and B for the Loma Prieta x-direction earthquake.

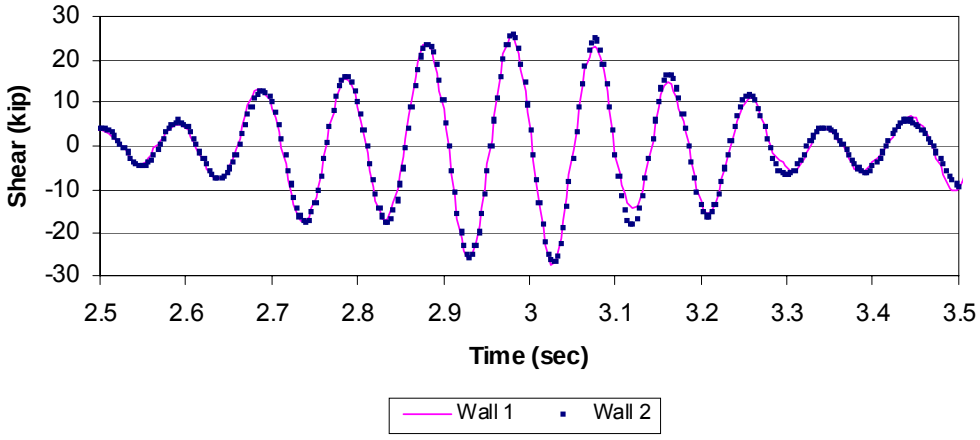

Figure 5-2. Base shears on walls 1 and 2 for the Loma Prieta y-direction earthquake.

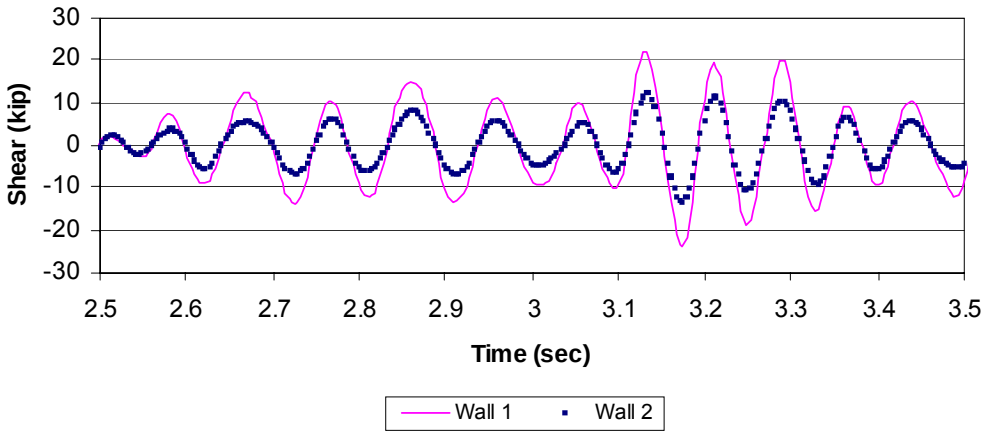

Figure 5-3. Effect of rigid diaphragm on wall 1 and 2 base shears (Loma Prieta y-dir).

When shear forces are acting on the in-plane walls, they deflect according to the force-deformation properties of the walls' constituent piers. From the earlier discussion it is known that, due to the flexibility of the diaphragms, the in-plane walls (in a given direction) will resist the same shear force. Thus, if the in-plane walls' deformation properties are not the same, the building will twist in accordance with the difference in deflection of the two walls. For the test model, the A-B plane direction is symmetric and, therefore, loading in that direction does not cause twisting. In the orthogonal direction, however, lateral loads will lead to twisting of the structure because wall 1 is considerably stiffer than wall 2 (see Figures 4-10 and 4-11). The twisting of the structure will create torsional shears that are resisted by the out-of-plane walls or, for this case, walls A and B. The induced shear forces in walls A and B must be in opposite directions to form a couple that counteracts the twist. This torsional behavior can be seen in Figure 4-6 by noting that the out-of-plane wall shear forces for x-direction motion are insignificant compared to that generated by loading in the y-direction.

Practically speaking, the twisting of the structure is of little concern for loading only in the 1-2 plane direction, because walls 1 and 2 would have to be pushed far past their capacity for the shears on walls A and B to do any sort of damage. For loading in the x and y direction, however, the addition of in-plane and torsional shears may initiate or increase structural damage; thus, an accurate description of building behavior is essential. As a result, only a 3D time-history analysis is suitable because it allows for an investigation of combinational effects at any time location throughout the duration of the ground motion. Figures 5-4 through 5-6 present the base shear on wall A for each of the earthquakes considered in Chapter 3 during the maximum demand on the structure.

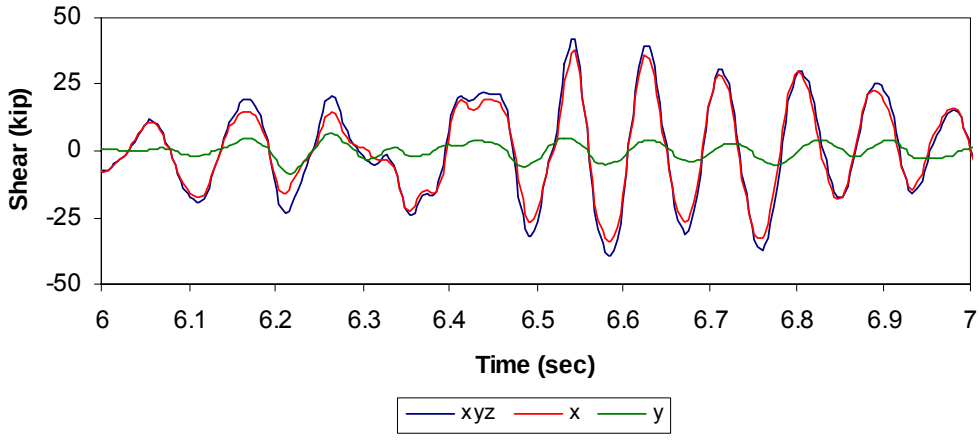

Figure 5-4. Base shear on wall A for Nahanni earthquake.

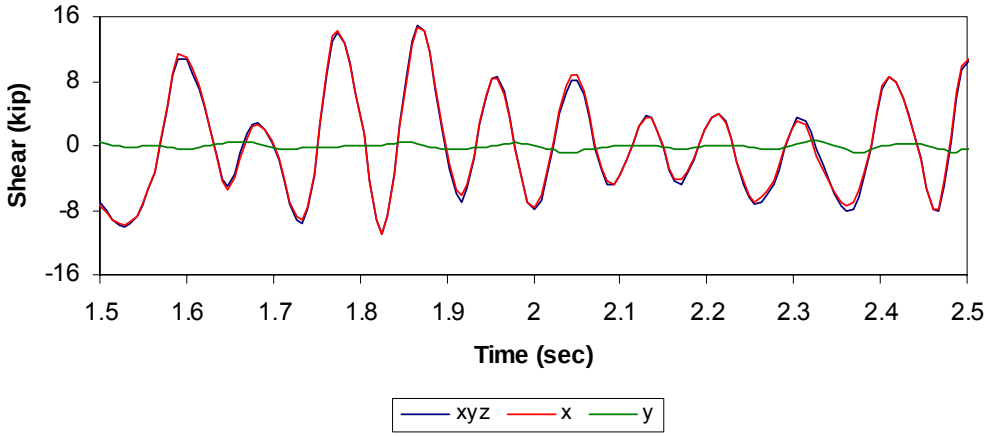

Figure 5-5. Base shear on wall A for El Centro earthquake.

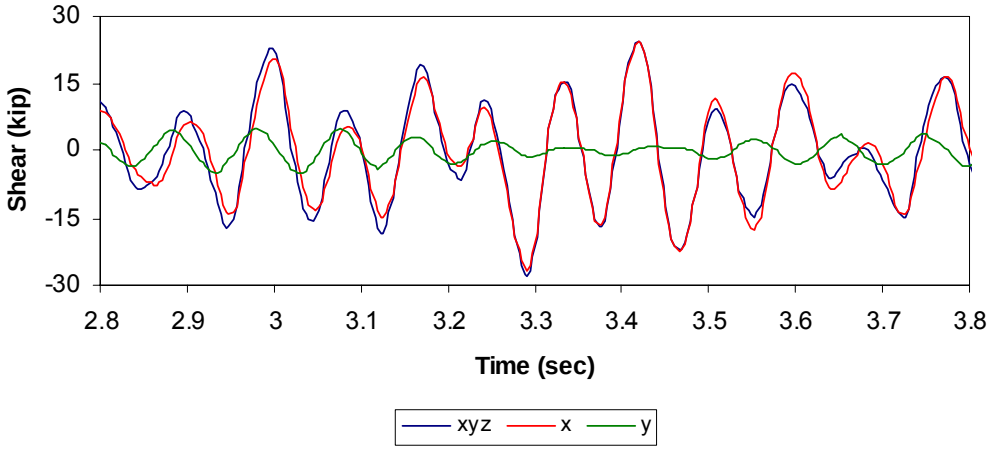

Figure 5-6. Base shear on wall A for Loma Prieta earthquake.

The figures indicate that there is a substantial base shear on wall A due to twisting of the structure (y component), and that the overall shear force under tri-directional excitation can be determined by summing the components due to x and y shaking (as would be expected for linear analysis). Figures 5-5 and 5-6 also show that, since orthogonal components of earthquake time-histories are different, the maximum shear due to twisting does not usually occur at the same time as the maximum shear due to in-plane loading. This fact is at the basis of the 100 percent-30 percent combination of maximum response quantities for orthogonal ground motions prescribed in FEMA 368. However, Figure 5-4, which is the base shear on wall A for the Nahanni earthquake, indicates that the maximum torsional shear *can* occur at the same time as the maximum in-plane shear. The implications of this result with respect to FEMA 368 are discussed later in this chapter.

It is important to understand that the twist of the structure that causes the combinations above is a result of the building responding in its fundamental mode. In other words, the fundamental mode shape for the test model has a slight twist in the 1-2 plane direction because of the relative differences in wall stiffness. There is no indication that the structure's torsional mode is affecting its dynamic response. Hypothetically, if the building did respond in a torsional mode the base shears would be affected to a much larger degree than what is shown in Figures 5-4 through 5-6.

Vertical Forces

Perhaps even more critical than the combinations of base shears for URM buildings are the effects of vertical compressions and tensions. For most other types of construction, the vertical compressive stress does not have a significant effect on the shear capacity of an element. As discussed in Chapter 3, however, this is not the case for masonry piers. Therefore, careful consideration of the changes in vertical compressive forces in URM buildings is required.

The majority of changes in vertical stress do not come from the vertical ground motions themselves, but rather from the lateral motions on the building. Masonry buildings constitute a box system, and that system is necessary to resist horizontal actions (Beskos and Anagnostopoulos 1997). Therefore, when the building experiences force in one direction, the in-plane walls resist the force by shear, and the connecting flanges of the out-of-plane walls resist the force by compression and tension. In this way, the out-of-plane walls help prevent the global overturning of the structure. This behavior is especially evident in a building like the test model, which has a small plan aspect ratio.

As seen in Figures 4-7 and 4-8, a large amount of compression and tension occur when the walls are loaded in a direction perpendicular to their length (cross-motion), e.g., when wall A experiences load from the y component. Sometimes these forces are enough to place the wall in tension (negative numbers in Figure 4-8). When the actual stress distribution in the wall is considered, it is evident that the majority of the compression or tension in an out-of-plane wall is located at its edges, where it acts as a flange to the connecting perpendicular walls (Figure 5-7). This might explain the extensive corner damage found in some URM buildings during post-earthquake investigations. For the Nahanni motion, the amount of flange tension is enough to crack the bases of the outside piers in walls A and B.

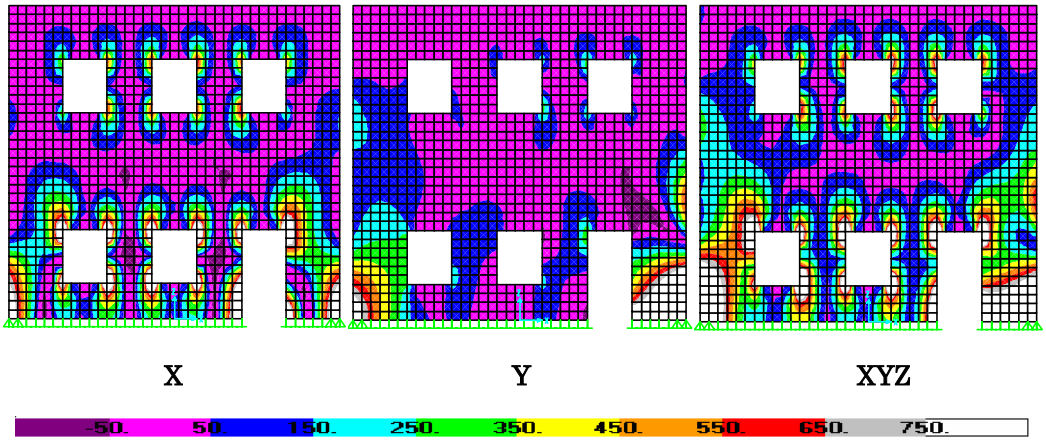

Figure 5-7. Vertical forces in wall A under Nahanni ground motion (pounds/inch).

In the interior portion of the wall, away from the regions affected by flange effects, the vertical stress diminishes. However, additional tensile stresses can occur in this region due to the deformation of the diaphragm. For example, consider the structure tested by Cohen (2001), which had plan dimensions of 22 ft by 4.67 ft. Finite element analysis indicated that a large area of vertical tension in the center of the out-of-plane wall developed as a result of bending (upper diagram in Figure 5-8). The maximum tensile stress occurs at the center of the wall because this point corresponds to the maximum point of diaphragm deflection. Testing confirmed this behavior when cracks appeared at the center of the base of the wall, allowing it to rock out-of-plane. Once the cracks formed, the wall could no longer carry tension (lower diagram in Figure 5-8).

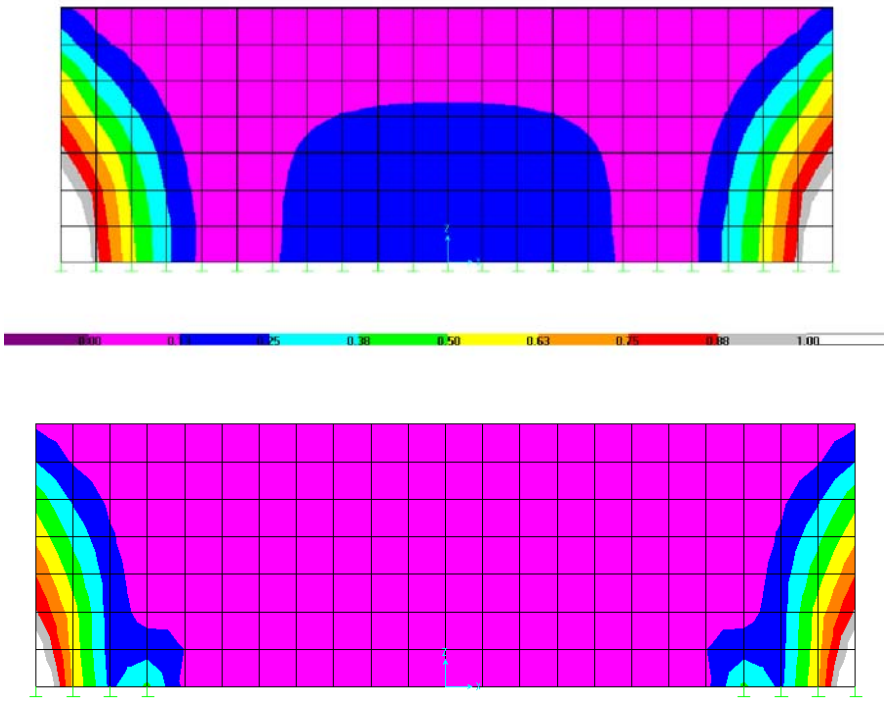

Figure 5-8. Vertical force contours for Cohen's structure under out-of-plane loading (kip/feet).

This behavior is not evident in the stress distributions of the test structure, primarily because it does not have a large enough plan aspect ratio. For longer structures like Cohen's, the center of the out-of-plane walls are located further away from the flange effects and the deformation of the diaphragm is much larger proportionally than the deformation of the shear walls.

The in-plane walls of the structure also develop vertical stresses as a result of lateral loading, as the first plot in Figure 5-7 demonstrates. The overturning moment caused by the lateral load induces compression on one side of the wall and tension on the other side. Large stress concentrations result at points of discontinuity in the walls, which could lead to cracking. Outside of these regions, the stresses are considerably smaller, especially in the center of the piers, because the piers primarily resist lateral load through shear.

Although the majority of vertical forces come from horizontal motions on the structure, there is some effect from the vertical component of the ground motion. As seen in Figures 4-7 and 4-8, the z component of the ground motions do increase and decrease the vertical forces on the walls by notable amounts. Generally, however, the figures indicate that the total vertical force in the walls for tridirectional excitation is controlled by the component perpendicular to the wall under consideration.

While Figures 4-7 and 4-8 are good indicators of the global response of the structure, they do not adequately address the local vertical effects of the various ground motion components. For instance, in-plane excitation induces compressions and tensions but, over the length of the wall, they sum to nearly zero. Consequently, it would appear that in-plane loading has no effect on the vertical loads in the wall even though this is clearly not the case. Moreover, the variation in vertical force along the length of a wall due to cross-motion also cannot be captured by Figures 4-7 and 4-8. Of the three directions of ground motion, only the z component has a relatively universal effect on the structure. To demonstrate the variation in vertical force along the length of a wall, Figures 5-9 and 5-10* plot the vertical force in piers 4 and 3 (wall A), respectively, under the Nahanni ground motion.

Figure 5-9 shows that, for pier 4, the dominant contributor to the 3D response is the y component, or the component perpendicular to wall A. This behavior is expected because pier 4 is located at the edge of wall A, where flange effects are considerable. In contrast, Figure 5-10 indicates that, for pier 3 (which is located near the center of wall A), both the z and y components have significant influence. At various points during the greatest period of shaking, the 3D response is controlled by either of these components. For both piers, the vertical force caused by the in-plane (x) ground motion is generally out of phase with the force due to the orthogonal (y) component, thus reducing the overall vertical force for the xyz ground motion.

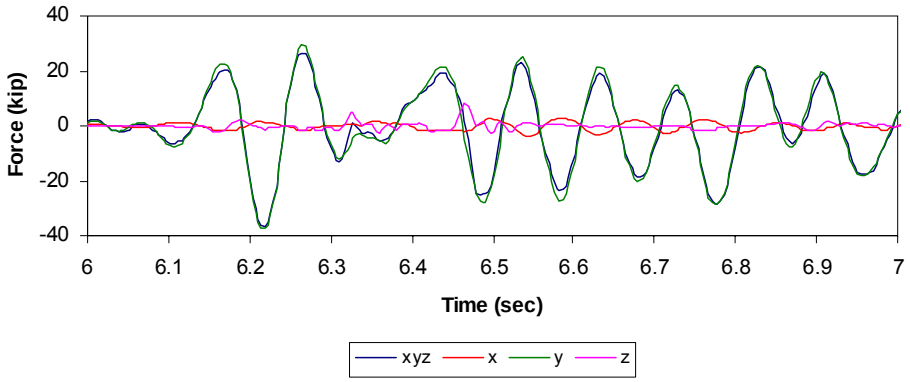

Figure 5-9. Vertical force in pier 4 (wall A) for the Nahanni ground motion.

* The vertical force plotted is due to earthquake forces only and does not include dead loads. See the bottom of Figure 4-7 for the forces in the walls caused by the dead load of the structure.

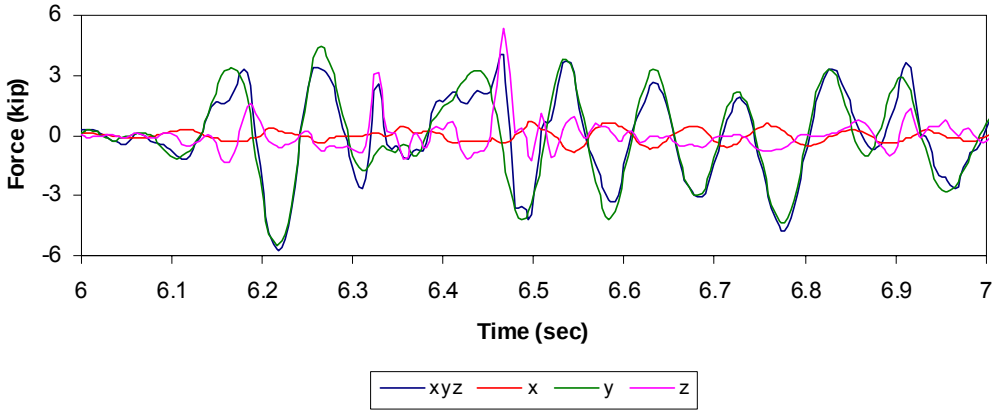

Figure 5-10. Vertical force in pier 3 (wall A) for the Nahanni ground motion.

Combined Shear and Vertical Forces

To determine the actual response of the masonry building system, the lateral shear forces and vertical forces must be considered together. The development of pier strengths in Chapter 3 clearly presented the dependency of strength on compressive stress. A large horizontal shear in conjunction with a tensile force could have catastrophic effects on the structure. To understand the effect of each ground motion on the building system, the interaction of the base shear and vertical force for wall 2 was examined. Figures 5-11 through 5-13* plot the response of the wall during peak demands for each earthquake (note that negative vertical forces are tensile forces).

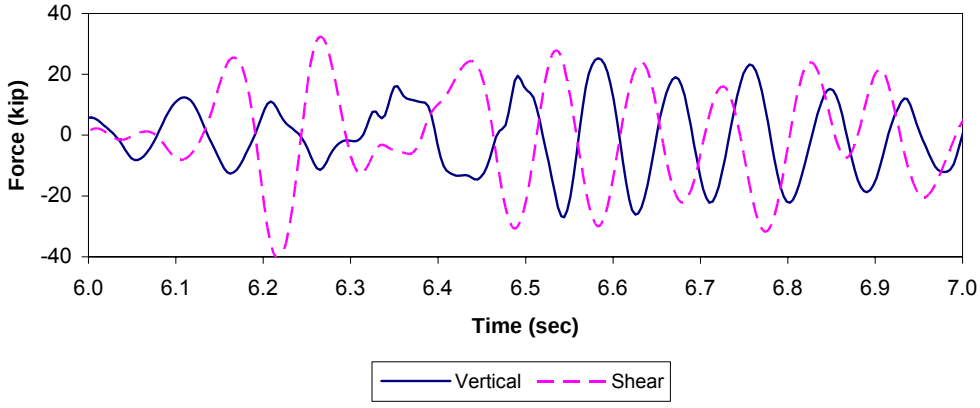

Figure 5-11. Combined shear and vertical forces on wall 2 under Nahanni ground motion.

* The vertical force plotted is due to earthquake forces only and does not include dead loads. See the bottom of Figure 4-7 for the forces in the walls caused by the dead load of the structure.

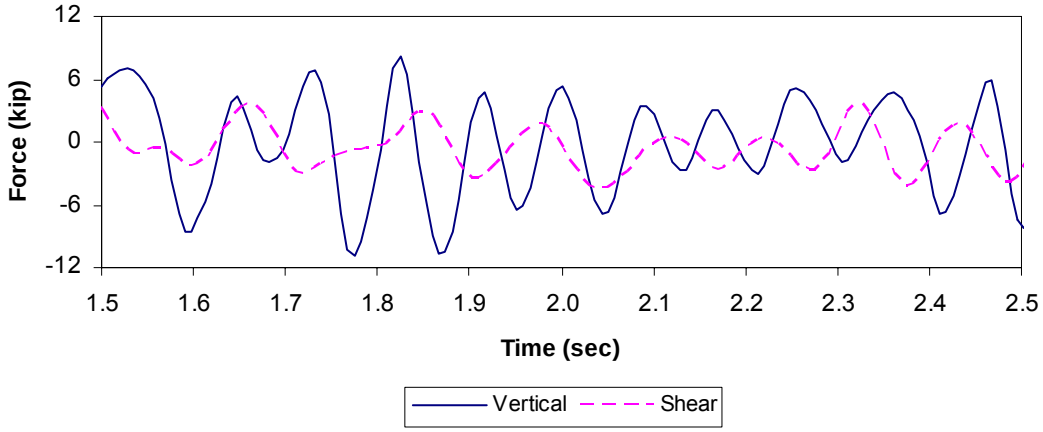

Figure 5-12. Combined shear and vertical forces on wall 2 under El Centro ground motion.

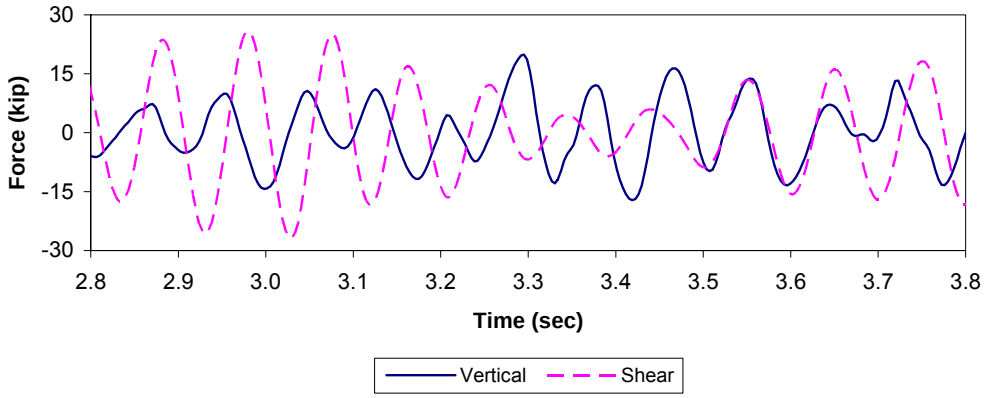

Figure 5-13. Combined shear and vertical forces on wall 2 under Loma Prieta ground motion.

As discussed in the previous section, vertical forces are due primarily to flange effects from excitation perpendicular to a given wall. Thus, the occurrence of large wall shears and vertical forces is actually an investigation of concurrent peak responses from orthogonal horizontal components. An examination of additive base shears in Figures 5-4 through 5-6 indicated that such combinations occurred for the Nahanni ground motion and not the Loma Prieta and El Centro earthquakes. Figures 5-11 through 5-13 confirm this conclusion demonstrating that, for the Nahanni earthquake, maximum tensile forces occur at the same time as near maximum base shears. While there are locations where vertical and shear forces combine for the other two earthquakes, they are not at points of maximum base shear, which are of primary concern.

The behavior of wall 2 in the above figures is indicative of the response of the other walls of the test structure, as would be expected. At any point in time, the in-plane walls for a given direction will sustain nearly the same base shear, but will resist vertical forces of opposite direction due to overturning. For the

Nahanni earthquake, therefore, the walls experience maximum shear and tension successively. Comparing the response of wall 1 to that of wall 2 exhibits this behavior (Figure 5-14*).

The Nahanni ground motion will greatly damage the building even without considering the vertical forces due to global overturning. Therefore, to understand the vertical impact, an analysis of the building with the Nahanni motion scaled down to 0.6 g† will be considered. At this level of acceleration, analysis done without considering the change in vertical load shows that the structure is not significantly damaged (no piers are rocking, Figure 5-15 (a)). The total shear on the wall is 8.0 kips while the shear required to start rocking is 9.3 kips. When the change in vertical load is considered, however, analysis indicates that the building is greatly damaged, Figure 5-15 (b). The corner piers go into tension, therefore having no rocking capacity according to FEMA 356. The inner piers lose about 1,000 lb of vertical force. Based on the present vertical stresses, the total shear capacity for the wall drops to 2.9 kips, much less than the 9.3 kips of shear the wall is experiencing. Note that the increased base shear is a result of the added twisting shear from the perpendicular ground motion component. With the consideration of vertical stress, wall A does not perform well.

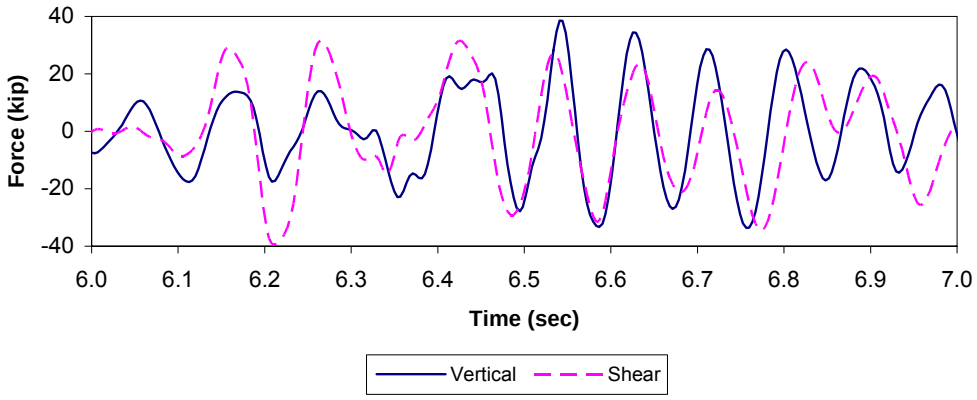

Figure 5-14. Combined shear and vertical forces on wall 1 under Nahanni ground motion.

* The vertical force plotted is due to earthquake forces only and does not include dead loads. See the bottom of Figure 4-7 for the forces in the walls caused by the dead load of the structure.

† g = the average acceleration produced by gravity

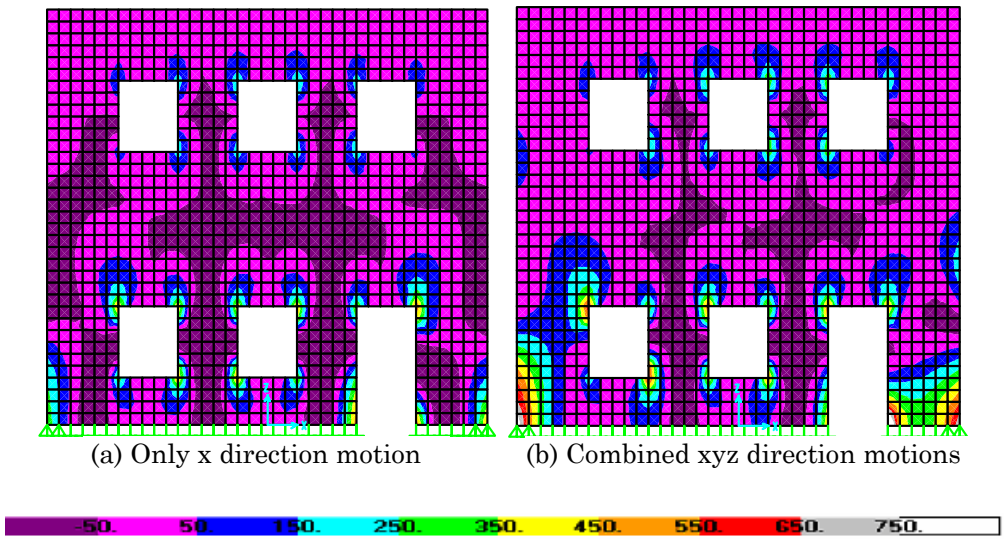

Figure 5-15. Comparison of vertical forces in wall A (pounds/inch).

Diaphragm Participation

The interaction between the diaphragm and the masonry walls also influences the behavior of the building system. One of the most evident changes is the change in natural frequencies from the 2D models that have no diaphragm effects, to the 3D model that includes the diaphragm (Table 5-1).

The fundamental periods of the structure are between the calculated periods for the diaphragm and the 2D walls. The increased period from the 2D models could possibly be attributed to two causes: the increased structural mass due to the diaphragm and out-of-plane walls and/or the effect of the diaphragm's flexibility. To determine the role of each, the 3D model was modified so that the diaphragm was essentially rigid while maintaining the same mass distribution. The resulting fundamental periods were 0.062 sec for A-B plane motion and 0.073 sec for 1-2 plane motion, still considerably smaller than the periods calculated in Table 5-1. Consequently, it appears that both the added mass and the diaphragm flexibility lengthen the response of the structure.

Table 5-1. Frequencies and periods for models

	2D model	3D model
Walls A&B	22.22 Hz, 0.045 sec	11.59 Hz, 0.086 sec
Wall 1	26.31 Hz, 0.038 sec	10.42 Hz, 0.096 sec
Wall 2	14.08 Hz, 0.071 sec	10.42 Hz, 0.096 sec
Diaphragm	8.8 to 16.7 Hz, 0.114 to 0.060 sec	

This could be just an aberration of the linear-elastic SAP model and may not happen in the real structure. However, Cohen (2001) found that his rectangular building behaved as a single degree of freedom system associated with the transverse response of the diaphragm. On the other hand, the aspect ratio of Cohen's structure is nearly five times that of the test model, and the effect of the diaphragm could be much less in this case. Only testing of the structure will determine the actual influence of the diaphragm's flexibility.

Besides changing the frequency of the building, the diaphragm has other effects on the building system. The base shears and deflections for the 3D model are greater than those for the 2D model. Again, these differences can likely be attributed to the dynamic influence of the diaphragm and the increased structural mass. Furthermore, as was discussed in Chapter 3, the out-of-plane wall demands are controlled by deformation of the diaphragm. This behavior can be observed in Figure 5-16, which presents the fundamental mode shapes of the structure. The figure also demonstrates the continuity between the out-of-plane walls and the diaphragm, which prevents the walls from falling out.

Calculated values of diaphragm deflection from the SAP model fell within the predicted values of deflection (Table 5-2). This result agrees with the conclusions from Chapter 3. Furthermore, combining the x and y components versus considering them independently made little difference in the diaphragm deflection in each direction.

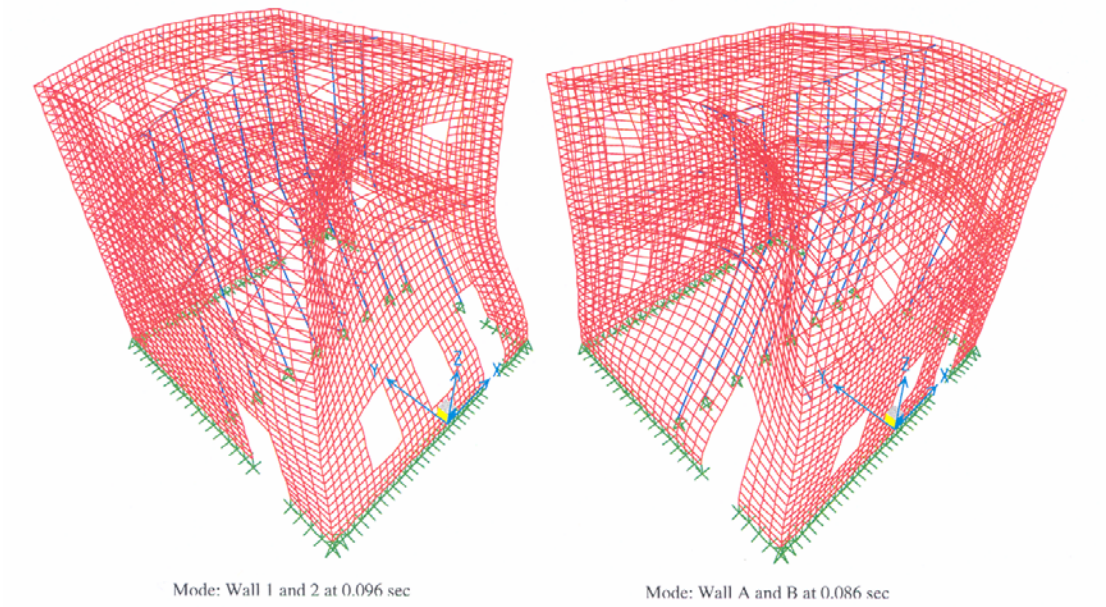

Figure 5-16. Fundamental modes of 3D test structure.

Table 5-2. Diaphragm deflections

		Displacement (in.)					
Diaphragm Shear (kip)		SAP		Cohen		FEMA 356	
x	y	x	y	x	y	x	y
5.18	5.132	0.1134	0.123	0.0453	0.0448	0.161	0.161
1.622	0.981	0.0448	0.023	0.0142	0.0086	0.0506	0.0306
2.473	2.02	0.0618	0.0802	0.0216	0.0176	0.0773	0.0631

Extrapolation of Component to System Behavior

The pushover analysis section in Chapter 4 showed that the individual force deformation relationships for the piers in a given wall can be combined to accurately determine the force deformation relationship for the wall (Figures 4-9 through 4-11). The section also demonstrated that the nonlinear response for the 3D building system follows the combined response of the 2D walls (Figures 4-12 and 4-13). However, the models did not allow for a change in pier strength due to a change in vertical load.

Previous discussions in this chapter indicated that the response of an out-of-plane wall depends on the flange effects from the in-plane wall. The two walls are connected to each other and influence each other's response. The lateral strength of a pier depends on its vertical load; thus, if the vertical load in a pier changes due to flange effects of connecting walls, the strength of the building may change.

The response of the structure is significantly affected by the properties of the diaphragm. As was stated in the previous section, the diaphragm deflection controls the demands on the out-of-plane walls. The flexibility of the diaphragm also controls the distribution of shear forces in the structure, which thereby controls the structural deformations. The 3-D analysis indicated that both the base shears and deflections were increased by the influence of the diaphragm, as were the fundamental periods.

Seismic Provisions

Earthquakes deliver the simultaneous application of load from three directions of ground motion. Standard practice considers each direction separately and then combines them using a combination rule. FEMA 368 states in Section 5.2.5.2, "The directions of application of seismic forces used in design shall be

those that produce the most critical load effects." The document goes on to say that, to determine the most critical load effects, loads may be applied independently in any two orthogonal directions and combined by considering 100 percent of the load in one direction and 30 percent of the load in the orthogonal direction. This combination is based on the principle that the earthquake response quantities in two orthogonal directions are unlikely to reach their maximum simultaneously. FEMA 356 and other building codes make similar combinations of independently applied loading.

Problems arise when maximums from orthogonal ground motion components occur at the same time because the total response is a 100 percent-100 percent combination as opposed to 100 percent-30 percent. If the combining quantities were of nearly the same value, there could be as much as a 35 percent underestimation. In the Chapter 5 discussion on base shears, it was discovered that the maximum base shears on wall A from the x and y components of the Nahanni earthquake did occur at the same time. Using the FEMA 368 prescription, the base shear is underestimated by 3.20 kip or 7.5 percent.

Even with the behavior of the test structure understood, the question remains as to how to predict such combinations in any URM building under any earthquake. Clearly, the more irregular the building, the more important twisting shears become. One way to alleviate the underestimation would be to run a time history analysis with ground motions applied in two or more directions simultaneously. This analysis can be accomplished with most structural analysis programs (e.g., SAP 2000NL). To run a time history analysis, however, a suite of ground motions is required, and these motions may not cause a directional combination. Neither the El Centro nor Loma Prieta ground motions caused the directional combination found in the Nahanni suite. Therefore, careful consideration of the time histories used in analysis is needed.

Response spectrum analysis does not use a time history of the ground motion; therefore, directional combinations may not be as evident. Nonetheless, their identification is necessary. The response spectrum procedure on wall A under the Nahanni motion calculated a base shear of 40 kips (Table 5-3). This is less than 42 kips determined from time-history analysis, but still more than the x direction component of 37 kips. In other cases, analysis overestimated the response. A better understanding is needed for when responses from orthogonal components of motion might combine.

Table 5-3. Comparison of response spectrum and time-history results for 3D model under simultaneous tri-directional loading

	Base Shear (kip)		Vertical force (kip)	
	response spectrum	time history	response spectrum	time history
Wall A	39.92	42.58	85.62/-49.86	65.17/-47.25
Wall B	40.62	33.86	86.74/-51.66	82.05/-39.90
Wall 1	41.47	31.51	50.57/-26.18	51.27/-21.53
Wall 2	42.42	32.56	36.70/-23.94	32.63/-21.04

In addition to the combination of in-plane base shears, seismic provisions also need to address the simultaneous action of lateral shears and vertical forces in a wall due to two or more orthogonal components of motion. As discussed previously, these forces can occur simultaneously, leading to decreased strength at times of maximum lateral load. The maximum base shear is caused by a component of motion acting parallel to the length of the wall, while the maximum vertical force comes from the component of motion acting perpendicular to the wall length. This effect is most evident in the corners where the vertical forces from flange effects are greatest. Seismic provisions should address the simultaneous action of two or more forces caused by different components of motion.

To accurately predict the concurrent action of forces, seismic provisions must also address the modeling requirements of the analysis procedures. FEMA 368 allows 2D models to be used for both the response spectrum and time history analysis procedures. These models are required to include the influence of diaphragm participation in the structural response, but not the influence of the flanges. As stated in previous sections, the flange effects from the out-of-plane walls do influence the behavior of the in-plane walls. Seismic provisions need to address the modeling requirements for structures whose lateral force resisting systems are not independent, such as in masonry buildings, in order to realize the simultaneous action of forces caused by different directions of motion.

Seismic provisions also give simple formulas to estimate the natural period of the building. The formulas in Section 5.4.2.1 of FEMA 368 are:

$$T_a = C_r h_n^{\,x} \qquad \text{Eq 5-1}$$

$$T_a = \frac{0.0019}{\sqrt{C_w}} h_n \qquad \text{Eq 5-2}$$

where h_n is the height of the building (11.78 ft), C_r is 0.02, and x is 0.75 for masonry buildings. C_w is 4.46 for walls A and B, and 3.03 for walls 1 and 2. The results of the equations are given in Table 5-4. The table shows that the FEMA 368 equations accurately approximated the periods within 0.04 sec. Although the code formulas may overestimate the period, they still can be used as an approximate method.

Table 5-4. Comparison of calculated and approximated natural periods (sec)

	3D FEM model	Equation 5-1	Equation 5-2
Walls A and B	0.086	0.127	0.0105
Walls 1 and 2	0.096	0.127	0.0128

6 Summary and Conclusions

Summary

This research was centered on a tri-axial analytical study of a half-scale URM structure. The test structure was developed cooperatively by U.S. Army ERDC-CERL and the Mid-America Earthquake Center. The objectives of the project focused on achieving a better understanding of the earthquake behavior of URM buildings. Specific objectives included:

- Investigate the effect of tri-directional base motions on the dynamic response of the structure.
- Examine dynamic amplification in systems with flexible diaphragms.
- Verify the extrapolation of individual component behavior to the overall response of the building system.
- Provide fundamental knowledge needed to develop seismic protection design.

The structure was analyzed based on the components of the structure and based on the whole building system. The masonry piers and wood diaphragms were analyzed to determine component behaviors. The building system was analyzed using equivalent static, response spectrum, linear time history, and pushover analysis. Each analysis method included careful consideration of the directions of load application. Seismic loads were applied independently along each coordinate axis and simultaneously along all three directions. Evaluations of the response of the building system under tri-directional loads were made.

Conclusions

Based on the objectives defined at the beginning of the report, specific conclusions can be made.

Objective 1 — *Investigate the effect of tri-directional base motions on the dynamic response of the structure.*

1. Combined horizontal motions can produce base shears larger than those resulting from independently applied motions. The combined responses can be larger than those predicted by the 100 percent-30 percent combination rule found in

FEMA 368. Combined responses become more critical for torsionally irregular buildings.

2. Vertical forces attracted to an out-of-plane wall are largely a result of global overturning of the building due to lateral motions. The vertical force is largest where an out-of-plane wall acts as a flange to an in-plane wall.
3. Vertical forces in a wall resulting from the vertical component of seismic motion can be significant, resulting in axial compression or tension proportional to the self-weight of the building.
4. Maximum in-plane base shears and vertical forces in a wall can occur at the same time, leading to decreased lateral strength at times of maximum base shear. This can cause increased damage in buildings whose lateral strength is sensitive to vertical load.

Objective 2 — *Examine dynamic amplification in systems with flexible diaphragms*

1. The fundamental response mode of the test structure is at a frequency consistent with the predicted in-plane deflection of the diaphragm.
2. For the test structure and the ground motions considered, flexibility of the diaphragm was shown to amplify the response of the walls.

Objective 3 — *Verify the extrapolation of individual component behavior to the overall response of the building system*

1. Force-deflection relationships for individual piers can be used to describe the force-deflection relationship of an in-plane wall, which can then be used to predict the response of the structure.
2. Response of an in-plane wall, especially the vertical forces attracted to the ends of a shear wall, is sensitive to the participation of the flanges.
3. The response of the diaphragm controls the demands on the out-of-plane walls by its deflection and also controls the demands on the in-plane walls through the distribution of lateral forces.

Objective 4 — *Provide fundamental knowledge needed to develop seismic protection design*

1. Combinations of lateral responses from orthogonal directions of motion should be investigated in determining design forces. Current formulations of the 100 percent-30 percent combination can underestimate the response.
2. Seismic provisions should address the interaction of responses resulting from separate ground motion components. Maximum in-plane base shears and vertical forces in a wall can occur at the same time, leading to decreased lateral strength at times of maximum base shear.
3. 2D modeling requirements for analysis need to consider the participation of wall flanges for masonry structures and other cases where the lateral force resisting systems are not independent.

4. Approximations for the structure's fundamental period found in FEMA 368 are similar to those calculated in analysis.

Recommendations

Based on the conclusions, the following recommendations are made:

1. Correlations need to be made between the analysis presented in this report and the measured response of the test structure under tri-axial dynamic testing.
2. Further studies should be done to quantify the effect of tri-directional motions on URM buildings of varying size and shape.
3. Further studies should be conducted to determine critical ground motion characteristics and structural features that lead to the direct combination of response quantities due to orthogonal earthquake components.
4. Studies should be conducted to quantify the flange effects of corner piers.
5. With the knowledge gained from this study, further studies should be conducted to determine how to effectively rehabilitate a building system.

References

American Forest and Paper Association. 1997. National Design Specification for Wood Construction (NDS).

Anastassiadis, K., Avramidis, I.E., and Panetsos, P. 2002. "Concurrent design forces in structures under three-component orthotropic seismic excitation," *Earthquake Spectra* **18**, 1-17.

Beskos, D.E., and Anagnostopoulos, S.A., ed. 1997. *Computer Analysis and Design of Earthquake Resistant Structures*, Computational Mechanics Publications, Boston.

Chopra, Anil. 1995. *Dynamics of Structures*, Prentice Hall.

Cohen, Gregory. 2001. *Seismic Response of Low-Rise Masonry Buildings with Flexible Roof Diaphragms*, Master Thesis, University of Texas at Austin.

Costley, A.C., and Abrams, Daniel. 1996. *Dynamic Response of Unreinforced Masonry Buildings with Flexible Diaphragms*, National Center for Earthquake Engineering Research Technical Report NCEER-96-0001.

Erbay, O., and Abrams, D.P. 2001. "Seismic rehabilitation of unreinforced masonry shear walls," *Proceedings 9th Canadian Masonry Symposium,* Fredericton, Canada.

Faherty and Williamson. 1999. Wood Engineering and Construction Handbook, 3rd edition, McGraw-Hill.

Federal Emergency Management Agency (FEMA). 1999. "Evaluation of Earthquake Damaged Concrete and Masonry Wall Buildings," FEMA 306, Washington, D.C.

_____. 2000. "Prestandard and Commentary for the Seismic Rehabilitation of Buildings," FEMA 356, Washington, D.C., November 2000.

_____. 2001. NEHRP Recommended Provisions for Seismic Regulations for New Buildings and Other Structures, Part 1 – Provisions, FEMA 368, Washington D.C.

_____. 2001. NEHRP Recommended Provisions for Seismic Regulations for New Buildings and Other Structures, Part 2 – Commentary, FEMA 369, Washington, D.C.

Harris, Harry, and Sabnis, Gajanan. 1999. *Structural Modeling and Experimental Techniques*, 2nd Edition, CRC Press.

Hwang, J., and Hsu, T. 2000. "Experimental study of isolated building under triaxial ground excitations," *Journal of Structural Engineering-ASCE* **126**:8, 879-886.

Lopez, O., Chopra, A.K., and Hernandez, J.J. 2001. "Evaluation of combination rules for maximum response calculation in multicomponent seismic analysis," *Earthquake Engineering and Structural Dynamics* **30**, 1376-1398.

Masonry Standard Joint Committee (MSJC). 1999. Building Code Requirements for Masonry Structures.

Orton, Sarah L. 2002. *Tri-Directional Seismic Response of Unreinforced Masonry Building Systems*, Masters Thesis, University of Illinois, Urbana-Champaign.

Pacific Earthquake Engineering Research (PEER) Strong Motion Database, June 2002, http://peer.berkeley.edu/smcat.

SAP2000 Non-Linear Version 7.40. 2000. Computers and Structures, Inc., Berkeley, CA.

Simsir, C.C., Aschheim, M.A., and Abrams, D.P. 2001. "Response of unreinforced masonry bearing walls situated normal to the direction of seismic input motions," *Proceedings 9th Canadian Masonry Symposium*, Fredericton, Canada.

Tena-Colunga, Arturo. 1992. Response of an Unreinforced Masonry Building During the Loma Prieta Earthquake, PhD Thesis, University of Illinois Urbana-Champaign.

Wilson, E.L., Der Kiureghian, A., and Bayo, E.P. 1981. "A replacement for the SRSS method in seismic analysis," *Earthquake Engineering and Structural Dynamics* **9** (2), 187-194.

REPORT DOCUMENTATION PAGE

Form Approved
OMB No. 0704-0188

1. REPORT DATE (DD-MM-YYYY)
04-2004

2. REPORT TYPE
Final

3. DATES COVERED (From - To)

4. TITLE AND SUBTITLE
Tri-Directional Seismic Analysis of an Unreinforced Masonry Building With Flexible Diaphragms

5a. CONTRACT NUMBER

5b. GRANT NUMBER

5c. PROGRAM ELEMENT NUMBER

6. AUTHOR(S)
Steven C. Sweeney, Matthew A. Horney, and Sarah L. Orton

5d. PROJECT NUMBER
622784AT41

5e. TASK NUMBER

5f. WORK UNIT NUMBER
008B40

7. PERFORMING ORGANIZATION NAME(S) AND ADDRESS(ES)
U.S. Army Engineer Research and Development Center (ERDC)
Construction Engineering Research Laboratory (CERL)
PO Box 9005
Champaign, IL 61826-9005

8. PERFORMING ORGANIZATION REPORT NUMBER
ERDC/CERL TR-04-6

9. SPONSORING / MONITORING AGENCY NAME(S) AND ADDRESS(ES)
U.S. Army Corps of Engineers
441 G Street, NW.
Washington, DC 20314-1000

10. SPONSOR/MONITOR'S ACRONYM(S)
CECW-EI

11. SPONSOR/MONITOR'S REPORT NUMBER(S)

12. DISTRIBUTION / AVAILABILITY STATEMENT
Approved for public release; distribution is unlimited.

13. SUPPLEMENTARY NOTES
Copies are available from the National Technical Information Service, 5285 Port Royal Road, Springfield, VA 22161.

14. ABSTRACT

To understand the susceptibility that buildings with flexible diaphragm systems have to earthquakes, their seismic response to tri-axial base motions is assessed. The research centers on a tri-directional analytical study of a two-story half-scale unreinforced masonry (URM) structure. It determines how individual component behavior, such as a pier or floor diaphragm, affects the behavior of the entire building system. This project achieves a greater understanding of the tri-directional seismic response of URM building systems with flexible diaphragms.

Analysis is conducted on the components of the structure and the building system. The masonry piers and the wood diaphragms are analyzed to determine component behaviors. The building system is analyzed using equivalent static, response spectrum, linear time history, and pushover analysis. Each analysis method includes careful consideration of the directions of load application. Seismic loads are applied independently along each coordinate axis and simultaneously along all three directions.

Evaluations of the response of the building system under tri-directional loads found that simultaneous tri-directional seismic motions do influence the response of the building system. Furthermore, the interconnectivity of walls in a masonry box building may cause significant changes in wall vertical forces due to global overturning of the building.

15. SUBJECT TERMS
unreinforced masonry
seismic studies
triaxial testing
structural reliability

16. SECURITY CLASSIFICATION OF:			17. LIMITATION OF ABSTRACT	18. NUMBER OF PAGES	19a. NAME OF RESPONSIBLE PERSON
					Steven C. Sweeney
a. REPORT	b. ABSTRACT	c. THIS PAGE			19b. TELEPHONE NUMBER (include area code)
Unclassified	Unclassified	Unclassified	SAR	94	(217)373-6798